A Douglas–Rachford Splitting Approach to Compressed Sensing Image Recovery Using Low-Rank Regularization

Shuangjiang Li, *Student Member, IEEE*, and Hairong Qi, *Senior Member, IEEE*

***Abstract*— In this paper, we study the compressed sensing (CS) image recovery problem. The traditional method divides the image into blocks and treats each block as an independent sub-CS recovery task. This often results in losing global structure of an image. In order to improve the CS recovery result, we propose a nonlocal (NL) estimation step after the initial CS recovery for denoising purpose. The NL estimation is based on the well-known NL means filtering that takes an advantage of self-similarity in images. We formulate the NL estimation as the low-rank matrix approximation problem, where the low-rank matrix is formed by the NL similarity patches. An efficient algorithm, nonlocal Douglas–Rachford (NLDR), based on Douglas–Rachford splitting is developed to solve this low-rank optimization problem constrained by the CS measurements. Experimental results demonstrate that the proposed NLDR algorithm achieves significant performance improvements over the state-of-the-art in CS image recovery.**

***Index Terms*— Compressed sensing, image recovery, nonlocal filtering, Douglas-Rachford splitting, low-rank estimation.**

I. INTRODUCTION

COMPRESSED Sensing (CS) has drawn quite some attention as a joint sampling and compression approach [1], [2]. It states that under certain conditions, signals of interest can be sampled at a rate much lower than the Nyquist rate while still enabling exact reconstruction of the original signal. CS-based approach has an attractive advantage that the encoding process is made signal-independent and computationally inexpensive at the cost of high decoding/recovery complexity. Usually, the CS measurement is acquired through projecting the raw signals on to a pre-defined random sampling operator. Thus, CS is especially desirable in some image processing applications when the data acquisition devices must be simple (e.g., inexpensive resource-deprived sensors), or when oversampling can harm the object being captured (e.g., X-ray imaging) [3], among which the compressive sensing Magnetic Resonance Imaging (CS-MRI) is most promising as it significantly reduces the acquisition time of MRI scanning. When applied to 2D images, CS faces several challenges including a computationally expensive reconstruction process and huge memory required to store the random sampling operator [4]. Several fast algorithms have been developed for CS reconstruction [4]–[6]. The memory challenge was first addressed in [7] using a block-based sampling operation, which later on became the most common method in CS image recovery.

Block-based compressed sensing (BCS) has made the CS image recovery practical since it reduces the recovery cost, where image acquisition is conducted in a block-by-block manner through the same compressed sensing (CS) measurement operator. However, manually dividing the image into blocks and treating each image block as an independent sub-CS recovery task would inevitably lose some global properties of the image. Thus it would often require some filtering technique (i.e., Wiener filter [4]) to generate good visual recovery result. Nonetheless, the recovered image still suffers a low PSNR. Aside from BCS, another class of popular methods is based on the total variation (TV) model [5], [8], which exploits the prior knowledge that a natural image is sparse in the gradient domain. TV based algorithms often suffer from undesirable staircase artifacts and tend to over-smooth image details and textures [9].

In this paper, we propose **NLDR**, a CS image recovery algorithm based on the BCS scheme. We overcome the aforementioned BCS problems by introducing a new nonlocal estimation step after the initial CS reconstruction to further remove noise. The nonlocal estimation process is built on the well-known nonlocal means (NL) filtering that takes advantage of self-similarities in images, which preserves certain global structure. We formulate the nonlocal estimation into the low-rank approximation problem where the low-rank matrix is formed by the nonlocal similarity patches. Furthermore, by using a deterministic annealing (DA) approach, we incorporate the CS measurement constraint into the low-rank optimization problem. We propose an efficient algorithm based on Douglas-Rachford splitting (DR) to solve the low-rank matrix approximation problem combined with the CS measurement constraints, the solution to which is the final CS recovery output. The proposed NLDR algorithm effectively reduces the staircase artifacts that introduced in BCS and TV by utilizing the nonlocal similarity patches while preventing over-smoothness by recursively incorporating the initial CS measurement constraint.

Manuscript received December 28, 2014; revised May 20, 2015; accepted July 16, 2015. The associate editor coordinating the review of this manuscript and approving it for publication was Dr. Quanzheng Li. *(Corresponding author: Shuangjiang Li.)*

The authors are with the Department of Electrical Engineering and Computer Science, University of Tennessee, Knoxville, TN 37996 USA (e-mail: sli22@vols.utk.edu; hqi@utk.edu).

Color versions of one or more of the figures in this paper are available online at http://ieeexplore.ieee.org.

Digital Object Identifier 10.1109/TIP.2015.2459653

The rest of the paper is organized as follows. Section II provides a brief review of the CS image recovery problem as well as some related works. Section III discusses the nonlocal estimation and Douglas-Rachford Splitting method. We conduct experiments in Section IV on both standard test images and MRI images. Section V concludes the paper.

II. Background and Related Works

A. CS Image Recovery Problem

Mathematically, the sparse representation model assumes that a signal $x \in \mathcal{R}^n$ can be represented as $x = \Psi\alpha$, where $\Psi \in \mathcal{R}^{n\times n}$ is a sparsifying basis or dictionary, and most entries of the coding vector α are zero or close to zero. This sparse decomposition of x can be obtained by solving a relaxed convex ℓ_1-minimization problem in the following Lagrangian form:

$$\min_{\alpha}\{\|x - \Psi\alpha\|_2^2 + \lambda_\alpha\|\alpha\|_1\}, \tag{1}$$

where constant λ_α denotes the regularization parameter.

In CS image recovery, we consider an image $I \in \mathcal{R}^{\sqrt{n}\times\sqrt{n}}$. By representing the image I in vector format, denoted as x, what we observe is the projected measurement y via $y = \Phi x + \nu$, where $\Phi \in \mathcal{R}^{m\times n} (m < n)$ is the measurement operator and ν is the additive noise vector. To recover x from y, first y is sparsely coded with respect to the basis Ψ by solving the following minimization problem

$$\hat{\alpha} = \arg\min_{\alpha}\{\|y - \Phi\Psi\alpha\|_2^2 + \lambda_\alpha\|\alpha\|_1\} \tag{2}$$

and then x is reconstructed by $\hat{x} = \Psi\hat{\alpha}$.

This can be easily extended to the block-based scenario, as stated in [10]. Let $x_i = R_i x$ denote an image patch extracted at location i, where R_i is the matrix extracting patch x_i from x at pixel location i. Given a basis Ψ, each patch can be sparse represented and solved by Eq. (1). Then the entire image x can be represented by the set of sparse code using $\{\Psi\alpha_i\}$. The patches can be overlapped to suppress the boundary artifacts.

Similarly, in order to reconstruct the image x from the measurement y, we can adopt the same block-based CS recovery by solving α_i from Eq. (2). The whole image x is then reconstructed as $\hat{x} = \Psi\hat{\alpha} = (\sum_i^N R_i^T R_i)^{-1}\sum_i^N (R_i^T\Phi\hat{\alpha}_i)$ as proved in [10].

The Iterative soft thresholding (IST) algorithm [11] can be very efficient in solving the problem in Eq. (2). In the $(k+1)$-*th* iteration, the solution is given by $\alpha^{(k+1)} = \mathcal{S}_\tau(\alpha^{(k)} + \Phi^* y - \Phi^*\Phi\Psi\alpha^{(k)})$, where $\mathcal{S}_\tau(\cdot)$ is the classic soft-thresholding operator [11]. In this paper, we use a slightly modified IST algorithm [12], where the solution in each iteration is called the *projected Landweber iteration* with the adaptive descent parameter $\beta^{(k)} > 0$,

$$\alpha^{(k+1)} = \mathcal{P}_{\mathcal{R}}[\alpha^{(k)} + \beta^{(k)}\Phi^*(y - \Phi\Psi\alpha^{(k)})], \tag{3}$$

where $\mathcal{P}_{\mathcal{R}}$ is the ℓ_2 projection of α on the ℓ_1 ball with radius $\mathcal{R}$. The adaptive descent parameter $\beta^{(k)}$ can be selected using the greedy strategy as follows,

$$\beta^{(k)} = \frac{\|\Phi^*(y - \Phi\Psi\alpha^{(k)})\|_2^2}{\|\Phi\Phi^*(y - \Phi\Psi\alpha^{(k)})\|_2^2} \tag{4}$$

This is an accelerated version of IST that converges faster than the original IST. Readers may refer to [12] for details.

B. Other Related Works

Buades et al. introduced in [13] the *nonlocal means* (NLM) filtering approach to image denoising, where the self-similarities between rectangular patches are used as a prior on natural images. The idea of nonlocal means has recently received much attention in image processing [14]–[19]. For example, Peyré et al. [14] proposed to use the Total Variation (TV) prior and nonlocal graph to solve the inverse problem with application in CS. The same idea was also adopted in Yang and Jacob [15]. Zhang et al. [16] proposed TVNLR which improves the conventional TV approach by adding a nonlocal regularization to the CS recovery problem and solved the problem using the Augmented Lagrangian Method (ALM). Shu et al. proposed the NLCS algorithm [17] and tried to group similar patches through NLS (nonlocal sparsity) regularization. The authors in [19] proposed a nonlocal total variation structure tensor (ST-NLTV) regularization approach for multicomponent image recovery from degraded observations, leading to significant improvements in terms of convergence speed over state-of-the-art methods such as the Alternating Direction Method of Multipliers (ADMM). Dong et al. proposed the nonlocal low-rank regularization (NLR-CS) method [18] which explored the structured sparsity of the image patches for compressed sensing. In order to explore the low-rank structure of the image patches, a smooth but non-convex surrogate function for the rank estimation is adopted as objective function. Zhang et al. proposed nonlocal TV regularization (NLVT) [20] for CS image recovery. NLTV is based on the Bregman iteration [21], namely Bregmanized Operator splitting (BOS).

In this paper, we adopt the nonlocal means filtering idea and introduce a new nonlocal estimation step after the initial CS reconstruction to further remove noise. It differs from [14] as we use the ℓ_1-norm based sparsity of the image and result in solving a convex optimization problem using the projection method. In [14] the nonlocal graph is similar to the nonlocal weights between patches as used in our paper. The main difference is that the author further imposed that these weights correspond to a probability distribution and that the graph only connects pixels that are not too far away. While in [15], the nonlocal weights may be improved using a different distance metric (i.e., robust distance metric) to promote the averaging of similar patches while minimizing the averaging of dissimilar patches. In this paper, we only aim to find similar patches to form low-rank matrix and thus differ from these methods. In [18] instead of using the nuclear norm for low-rank approximation, the authors proposed to use non-convex surrogate function and subsequently solved the optimization problem via ADMM.

In [17], two non-local sparsity measures, i.e., non-local wavelet sparsity and non-local joint sparsity, were proposed to exploit the patch correlation in NLCS. It then combines with the conventional TV measure to form the optimization objective function and use the ADMM method to solve the CS recovery problem. It differs from our algorithm in that their search for similar patches is incorporated in the objective function while NLDR directly adopts the nonlocal means filtering approach to find the similar patches and then conducts low-rank approximation. After getting the non-local low-rank estimation, we further incorporate the initial CS measurement constraint into the low-rank optimization problem, using a deterministic annealing (DA) approach to further improve the recovery result. Additionally, compared to the traditional ADMM method, we propose to use Douglas-Rachford splitting method to effectively solve the combined optimization problem.

In [22], Candès and Tao proposed to solve the matrix completion problem using low-rank regularization through convex optimization. Later in [23] Dong et al. first combined the nonlocal image representation and low-rank approach for image restoration and achived state-of-the-art performance in image denosing. Ji et al. [24] also incorporated the low-rank matrix completion in video denoising.

To summarize, the main contribution of this paper is three-fold: First, we propose to incorporate the nonlocal similarity patches searching step after the initial CS image recovery task. By searching and incorporating the nonlocal similarity patches the traditional block based CS recovery artifacts could be resolved. Second, we propose to estimate the grouped similarity patches matrix as a low-rank matrix completion problem, referred as nonlocal low-rank estimation. The idea is that, by searching the nonlocal similarity patches we could resolve the block and staircase artifacts, while using low-rank estimation we can further denoise the grouped similarity patches. Third, we incorporate the initial CS measurement constraint into the low-rank estimation optimization problem. By using a deterministic annealing (DA) approach, the Douglas-Rachford splitting effectively solves the reformulated optimization problem.

III. Nonlocal Low-Rank Regularization and Douglas-Rachford Splitting

In this section, we present the idea of nonlocal low-rank regularization, followed by the proposed Douglas-Rachford splitting method. We refer to the algorithm as the Nonlocal Douglas-Rachford splitting (NLDR) algorithm.

A. Nonlocal Low-Rank Regularization for CS Image

An example to illustrate the nonlocal estimation step is shown in Fig. 1. The *Lena* image in the first row is obtained from the IST CS recovery algorithm. Then the nonlocal similar patches are searched across the entire image. We denote the nonlocal similar patches of x_i as $x_{i,1}, x_{i,2}, x_{i,3}, \cdots x_{i,q}$. These extracted patches then form the matrix B_i where the low-rank approximation is conducted to yield the resulting denoised patch matrix, as shown in the second row. We apply patch reweight to obtain the estimated patch x_e to update the original patch x_i. After iterating over the entire image, the much cleaner *Lena* image is shown leftmost in the second row.

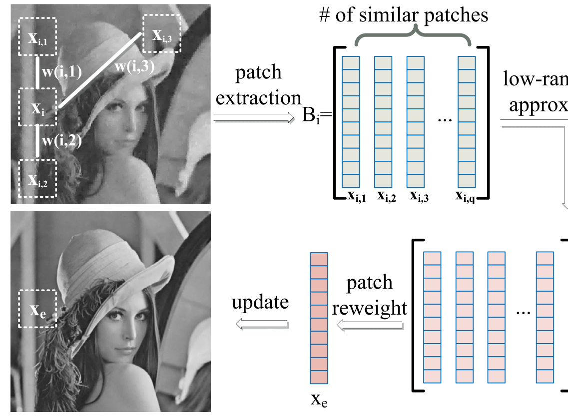

Fig. 1. An illustration of nonlocal estimation and similar patches denoising using low-rank matrix approximation.

1) Nonlocal Similarity Patches: The basic idea of nonlocal (NL) means filtering is simple. For a given pixel u_i in an image x, its NL filtered new intensity value, denoted by $NL(u_i)$, is obtained as a weighted average of its neighborhood pixels within a search window of size w.

In our work, we extend the pixel-wise nonlocal filtering to the patch-based filtering. Specifically, we search for the nonlocal similar "patches" $x_{i,j}$, $j = 1, 2, \cdots, q$, to the given patch x_i in a large window of size w centered at pixel u_i. Here, q is the total number of similar patches to be selected. The weight of patch $x_{i,j}$ to x_i, denoted as ω_{ij}, is then computed by

$$\omega_{ij} = \frac{1}{c_i} \exp\left(\frac{-\|x_i - x_{i,j}\|_2^2}{h^2}\right), \quad j = 1, \cdots, q \tag{5}$$

where h is a pre-determined scalar and c_i is the normalization factor. Accordingly, for each patch x_i, we have a set of its similar patches, denoted by $\mathbf{\Omega}_i$. Then the nonlocal estimates of each patch $\hat{x}_i$ can be computed as $\hat{x}_i = \sum_{j \in \Omega_i} \omega_{ij} x_{i,j}$. Further, this can be written in a matrix form as

$$\hat{x}_{nl} \doteq \mathbf{W} \sum_{i=1}^{p} \hat{x}_i, \quad \mathbf{W}(i, j) = \begin{cases} \omega_{ij}, & \text{if } x_j \in \Omega_i \\ 0, & \text{otherwise.} \end{cases} \tag{6}$$

where p denotes the number of all patches in the entire image and $\hat{x}_{nl}$ is the nonlocal estimated image output.

2) Patch Denoising by Low-Rank Approximation: Although we can use Eq. (6) to remove noise in the IST recovered image $\hat{x}$ to a certain degree, this is based on a weighted average of patches in $\hat{x}$, which are inherently noisy. Thus, it is imperative to apply some denoising techniques before the nonlocal similarity patch reweight using Eq. (6) to prevent the noise from accumulating. By rewriting the nonlocal similarity patches into the matrix format, we have $B_i = [x_{i,1}; x_{i,2}; , \cdots ; x_{i,q}]$, where each column of B_i is a vector representation of $x_{i,j}$, $j = 1, 2, \cdots, q$ for patch x_i. Since all columns of B_i share similarity with patch x_i, the columns of B_i should bear a high degree of similarity between each other. In other words, we can safely treat B_i as a low-rank matrix. We thus formulate the nonlocal patch denoising problem into the low-rank matrix approximation problem [22] as follows,

$$\min_{\hat{B}_i} \frac{1}{2}\|B_i - \hat{B}_i\|_2^2 + \lambda_{B_i}\|\hat{B}_i\|_*, \tag{7}$$

where $\|\hat{B}_i\|_*$ is the nuclear norm of the low-rank approximated patch matrix $\hat{B}_i$, defined by $\|\hat{B}_i\|_* \triangleq \text{trace}(\sqrt{\hat{B}_i^{\,T}\hat{B}_i}) = \sum_{r=1}^{q}\sigma_r$, and σ_r's are the singular values of $\hat{B}_i$.

In addition, since the columns of B_i (or the patches) are also a subset of the reconstructed image from IST recovery algorithm, it should be subject to the CS measurement constraint $y = \Phi x$. Therefore, multiplying Eq. (7) with $\mathbf{W}$, we reformulate the denoising problem of Eq. (7) into

$$\min_x \frac{1}{2}\|x - \mathbf{W}B_i\|_2^2 + \lambda_x\|x\|_* \text{ s.t. } y = \Phi x. \tag{8}$$

In what follows, we discuss in sec. III-B how to solve Eq. (8) with the CS measurement constraint using the method referred to as the Douglas-Rachford splitting method.

B. Douglas-Rachford Splitting

The Douglas-Rachford splitting method was originally proposed in [25] for solving matrix equations. Later on it was advanced as an iterative scheme to minimize the functions of the form,

$$\min_x F(x) + G(x) \tag{9}$$

where both F and G are convex functions for which one is able to compute the proximal mappings $\mathsf{prox}_{\gamma F}$ and $\mathsf{prox}_{\gamma G}$ which are defined as

$$\mathsf{prox}_{\gamma F}(x) = \arg\min_y \frac{1}{2}\|x - y\|_2^2 + \gamma F(y) \tag{10}$$

The same definition applies to $\mathsf{prox}_{\gamma G}$ [26]. In order to solve Eq. (8), we have $F(x) = \iota_{\mathcal{C}}(x)$ and $G(x) = \|x\|_*$, where $\mathcal{C} = \{x : y = \Phi x\}$ and $\iota_{\mathcal{C}}$ is the indicator function.

Given that $F(x) = \iota_{\mathcal{C}}(x)$, the solution to Eq. (10) is the same as projections onto convex sets (POCS), and does not depend on γ. Therefore, we have

$$\mathsf{prox}_{\gamma \iota_{\mathcal{C}} F}(x) = \mathsf{prox}_{\iota_{\mathcal{C}} F}(x) = x + \Phi^+(y - \Phi x), \tag{11}$$

where $\Phi^+ = \Phi^T(\Phi\Phi^T)^{-1}$ is the pseudoinverse of Φ. The proximal operator of $G(x)$ is the soft thresholding of the singular values

$$\mathsf{prox}_{\gamma G}(x) = U(x)\cdot\rho_{\lambda_x}(S(x))\cdot V(x)^* \tag{12}$$

where $x = U\cdot S\cdot V^*$ is the singular value decomposition of the matrix x and $S = \text{diag}(s_i)_i$ is the diagonal matrix of singular values s_i, and $\rho_{\lambda_x}(S)$ is defined as a diagonal operator.

$$\rho_\lambda(S) = \text{diag}(\max(0, 1 - \lambda_x/|s_i|)s_i)_i \tag{13}$$

We can then solve the problem in Eq. (7) using the Douglas-Rachford iterations given by

$$\tilde{x}_{k+1} = (1 - \frac{\mu}{2})\tilde{x}_k + \frac{\mu}{2}\mathsf{rprox}_{\gamma G}(\mathsf{rprox}_{\gamma F}(\tilde{x}_k)) \tag{14}$$

and the $(k+1)$-*th* solution $\hat{x}_{k+1}$ is calculated by $\hat{x}_{k+1} = \mathsf{prox}_{\gamma F}(\tilde{x}_{k+1})$. Here the reversed-proximal mappings is given by $\mathsf{rprox}_{\gamma F} = 2\mathsf{prox}_{\gamma F} - x$ for $F(x)$ and in the similar fashion to G(x).. The parameters are selected as $\lambda_x > 0$ and $0 < \mu < 2$ which guarantee $\hat{x}$ to be a solution that minimizes $F(x) + G(x)$ based on the proof in [27].

Algorithm 1 Nonlocal Douglas-Rachford Splitting (NLDR) Algorithm

Input:
- ► Measurement matrix $\Phi \in \mathbb{R}^{m\times n}$
- ► Basis matrix $\Psi \in \mathbb{R}^{n\times n}$
- ► Observation vector $y \in \mathbb{R}^m$.
- ► Number of IST iterations iter, number of nonlocal estimation iterations J, DR splitting iterations K

Output:
- ► An estimate $\hat{x} \in \mathbb{R}^n$ of the original image x.

```
Initialize α^0 ← 0
for k = 1, ··· , iter do
    (a) Select β^(k) based on Eq. (4)
    (b) Update α^(k+1) using Eq. (3)
end for
for j = 1, 2, ··· , J do
Step 1: Nonlocal Estimate
    (a) Calculate nonlocal weights ω_ij via Eq. (5)
    (b) Obtain low-rank patch matrix B_i via Eq. (7)
Step 2: Douglas-Rachford Splitting to solve Eq. (8)
    for k = 1, 2, ··· , K do
    (a) Calculate prox_γF(x) via Eq. (11)
    (b) Calculate prox_γG(x) via Eq. (12)
    (c) Calculate x̃_(k+1) via Eq. (14)
    end for
end for
return x̂ ← x̃_(k+1)
```

C. The NLDR Algorithm

Algorithm 1 provides a pseudo-code for the proposed Nonlocal Douglas-Rachford splitting (NLDR) algorithm. Given the observation y (i.e., compressed measurements), the NLDR algorithm first outputs an intermediate reconstruction result $\hat{x}_{IST}$ through the IST algorithm. This soft-thresholding output is then used to calculate the nonlocal estimated image $\hat{x}_{nl}$, which is used to initialize the low-rank optimization problem in Eq. (7) where the Douglas-Rachford splitting method will be carried out iteratively based on Eq. (14).

As for calculating the nonlocal estimates of the image, the NLDR algorithm obtains the averaged result based on J nonlocal estimation iterations. For the IST algorithm, we empirically set the penalty parameter $\lambda_\alpha = 1.8$ and soft-thresholding parameter $\tau = 1.2$, respectively.

IV. Experiments

In this section, we evaluate the NLDR algorithm for CS image reconstruction where both standard test images and MRI images are used. The reason for choosing MRI images for evaluation purpose is due to the significant impact of CS on the clinical practice of MRI, where long acquisition time

TABLE I

PSNR PERFORMANCE IN dB

Images		Lena											
Algorithms		IST	TV	TVAL3	BCS-SPL	IST+BM3D	NLCS	TVNLR	NLR-CS	NLTV	NLDR	TVAL3+NLDR	BCS-SPL+NLDR
m/n	0.1	25.41	22.75	29.02	28.31	25.93	31.74	28.62	29.58	25.94	33.67	**33.81**	33.80
	0.2	29.57	24.44	31.56	31.37	30.42	34.78	30.98	32.95	29.73	36.33	**36.35**	**36.35**
	0.3	32.05	25.47	32.99	33.50	32.91	36.67	33.52	34.73	31.73	37.82	**37.83**	**37.83**
	0.4	34.07	27.88	35.03	35.20	34.72	38.22	35.48	36.56	35.39	**39.02**	**39.02**	**39.02**
	0.5	35.89	30.73	36.26	36.79	36.34	39.66	36.94	38.77	37.90	40.16	**40.17**	40.16
		Barbara											
m/n	0.1	21.18	20.10	21.31	22.85	21.34	24.34	22.55	26.90	23.13	29.48	**31.14**	31.01
	0.2	24.35	21.66	21.60	24.33	24.80	28.17	24.30	30.87	28.29	**35.28**	35.21	35.22
	0.3	26.96	23.61	24.79	25.92	27.73	31.65	25.35	34.26	31.79	37.30	37.30	**37.32**
	0.4	29.38	25.32	28.55	27.68	30.29	34.32	26.85	36.14	34.44	**38.95**	**38.95**	**38.95**
	0.5	31.73	26.62	31.08	30.15	32.82	36.63	28.02	39.36	36.23	40.50	**40.51**	**40.51**
		Peppers											
m/n	0.1	24.30	21.98	29.69	28.88	24.77	31.85	26.25	29.18	25.78	32.91	**33.11**	33.07
	0.2	29.16	23.47	32.70	31.44	29.86	33.99	31.64	32.38	29.35	**34.74**	34.70	34.69
	0.3	31.54	25.57	34.02	32.89	32.16	35.27	34.35	33.73	32.85	**35.78**	35.70	35.70
	0.4	33.29	27.56	34.98	34.06	33.57	36.41	35.62	35.29	34.82	**36.91**	36.75	36.75
	0.5	34.73	29.67	36.08	35.18	34.57	37.52	36.74	37.03	36.96	**38.13**	37.99	37.99
		Mandrill											
m/n	0.1	19.68	19.79	19.01	20.21	19.66	20.89	20.37	20.63	19.95	21.15	**21.89**	21.80
	0.2	21.02	21.17	19.22	21.09	20.69	22.78	21.93	21.89	22.25	23.43	**24.08**	23.93
	0.3	22.34	22.81	19.70	21.80	21.79	24.44	23.11	23.21	24.64	25.49	**25.85**	25.73
	0.4	23.68	24.79	20.20	22.92	23.13	26.17	24.26	25.20	26.95	27.47	**27.91**	27.81
	0.5	25.16	26.71	22.73	24.50	24.72	27.87	25.42	27.16	29.37	29.40	**29.71**	29.66
		Goldhill											
m/n	0.1	24.96	22.56	27.45	26.96	25.08	28.53	25.20	28.92	23.58	28.94	**29.66**	29.57
	0.2	27.81	23.93	29.86	28.95	27.87	30.84	28.92	31.60	26.90	32.10	**32.26**	32.24
	0.3	29.53	25.88	31.62	30.56	29.49	32.55	31.29	33.37	30.08	33.99	**34.02**	**34.02**
	0.4	31.23	27.73	33.21	32.09	30.92	34.13	33.08	34.36	32.66	35.61	**35.63**	35.62
	0.5	32.76	29.44	33.29	33.61	32.18	35.67	34.55	36.41	35.01	37.20	37.20	**37.21**
		Cameraman											
m/n	0.1	23.86	22.05	28.50	26.36	24.38	33.26	25.53	30.72	29.71	36.83	**36.97**	36.85
	0.2	26.97	24.11	34.12	30.07	31.66	37.49	30.67	35.29	33.95	41.49	**41.56**	41.55
	0.3	33.66	26.55	38.16	32.82	35.44	40.71	34.34	37.79	37.65	43.92	**43.96**	**43.96**
	0.4	34.85	29.23	40.42	35.48	38.28	43.40	37.56	41.65	40.83	45.96	**46.01**	45.95
	0.5	36.26	34.02	43.01	37.85	40.71	45.92	39.95	45.56	43.67	47.90	**47.92**	47.90
		Boat											
m/n	0.1	23.77	21.48	25.76	24.65	24.16	27.74	24.03	26.41	23.94	28.69	**29.52**	29.24
	0.2	27.01	23.18	28.94	27.02	27.38	30.66	28.02	29.07	27.97	32.48	**32.68**	32.63
	0.3	29.10	24.84	31.09	28.94	29.61	32.64	30.80	30.65	30.89	34.41	**34.47**	34.43
	0.4	30.91	26.93	32.68	30.59	31.24	34.26	33.06	32.48	33.45	35.77	35.81	**35.86**
	0.5	32.68	29.19	33.53	32.19	32.76	35.73	34.66	35.87	36.04	37.24	37.24	**37.25**

has been one of the primary obstacles. We implement the algorithm using *Matlab* 2013b on a 2.20GHz laptop computer. BCS-SPL [4] is a block-based CS image recovery method solved using a smoothed version of projected Landweber (SPL) algorithm. The smoothing process is done by the Wiener filter. We further compare our result with one of the state-of-the-art algorithms for image CS recovery, known as TVAL3 [6]. TVAL3 tries to minimize the image total variation norm using augmented lagrangian and alternating direction algorithms. Several TV-based methods are also compared. The TV benchmark method denoted as TV which is implemented based on [28], TVNLR [29] and NLTV [20]. We also compare NLDR performance with other nonlocal based approaches, e.g., NLCS [17] and NLR-CS [18]. Finally, to evaluate the potential of NLDR as a standalone denoising method, we compare its performance with the state-of-the-art BM3D [30] method for noise removal purpose.

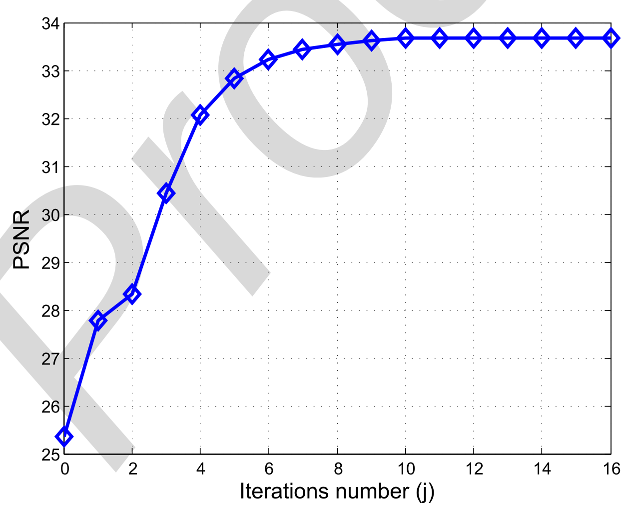

Fig. 2. CS recovery results on *Lena* image with 10% measurements at iteration j.

AQ:2

A. CS Recovery on Standard Image Dataset

We present the experimental results for noiseless CS measurements and then report the results using noisy CS measurements.

1) Noiseless Recovery: We first test the NLDR algorithm in noiseless settings using standard test images of size 512×512. The block-based image patch is of size 6×6. We set the number of similar patches q in the nonlocal

Fig. 3. CS Reconstructed image *Barbara* with 30% measurement ratio. (a) Original image; (b) proposed **NLDR** recovery, PSNR = 37.30dB; (c) BCS-SPL recovery [4], PSNR = 25.92dB; (d) TVAL3 recovery [6], PSNR = 24.79dB; (e) TVNLR recovery [29], PSNR = 25.35dB. (f) NLCS recovery [17], PSNR = 31.65dB; (g) NLR-CS recovery [18], PSNR = 34.26dB; (h) NLTV recovery [20], PSNR = 31.79dB.

Fig. 4. *Boat* image with cropped character patch using 20% measurements. (a) proposed **NLDR** recovery, PSNR = 32.48dB; (b) NLCS recovery [17], PSNR = 30.66dB; (c) TVNLR recovery [29], PSNR = 28.02dB; (d) NLR-CS recovery [18], PSNR = 29.07dB; (e) NLTV recovery [20], PSNR = 27.97dB.

Fig. 5. Part of *Lena* image with 200% magnification using 20% measurements. (a) Original image; (b) reconstruction using proposed NLDR with IST, PSNR = 36.33dB; (c) TVAL3 + NLDR, PSNR = 36.35dB (d) BCS-SPL + NLDR, PSNR = 36.35dB.

estimation step as 45. We use the scrambled Fourier matrix as the CS measurement operator Φ and DCT matrix as the basis Ψ to represent the original image in the initial IST recovery. The parameters are selected as $\mu = 1$ for DR iteration and $\lambda_x = \frac{c_i}{\max(s_i)}$ for each iteration where $c_i = C_0 * \epsilon, 0 < \epsilon < 1$ and C_0 is a constant. For the number of iterations in the outerloop, we find that the recovery result gradually converges when J reaches 12 for all the image datasets. Fig. 2 shows one example on *Lena* image using 10% of measurements. Note that at iteration 0, we use the initial IST recovery result.

Table I compares PSNR with different measurement ratios (i.e., $\frac{m}{n}$). We see that the NLDR algorithm considerably

TABLE II

CS Noisy Recovery Results on Standard Test Images With 20% Measurements

	Algorithm								
	NLDR	**TV**	**NLTV**	**BCS-SPL**	**TVAL3**	**TVNLR**	**NLCS**	**NRL-CS**	**BM3D**
SNR	**Lena**								
5	36.24	21.27	25.94	30.50	28.82	28.14	32.45	32.55	30.32
10	36.29	21.63	27.66	30.51	28.93	28.43	33.13	32.65	30.31
15	36.29	22.19	28.34	30.52	30.94	29.23	33.44	32.76	30.31
25	36.29	23.63	29.01	30.52	31.18	30.96	34.01	32.90	30.34
35	36.29	24.34	29.50	30.52	31.18	30.98	34.57	32.95	30.34
Noiseless	36.33	24.44	29.73	31.37	31.56	30.98	34.78	32.95	30.42
	Barbara								
5	35.15	19.03	25.11	24.40	19.45	23.22	27.73	30.39	24.74
10	35.16	19.34	25.94	24.44	19.80	23.56	27.86	30.50	24.75
15	35.16	19.87	26.37	24.45	19.94	24.17	28.02	30.76	24.77
25	35.21	21.05	27.35	24.45	20.03	24.04	27.94	30.87	24.77
35	35.27	21.32	28.04	24.46	20.07	24.28	28.01	30.87	24.80
Noiseless	35.28	21.66	28.29	24.33	21.60	24.30	28.17	30.87	24.80
	Peppers								
5	34.61	20.11	26.21	30.77	31.33	29.87	32.11	32.01	29.79
10	34.61	20.49	26.73	30.77	31.71	30.01	32.49	32.17	29.73
15	34.68	21.61	27.01	30.92	31.99	30.55	33.41	32.30	29.76
25	34.68	23.20	28.35	30.92	32.66	31.60	33.37	32.38	29.80
35	34.58	23.44	29.22	30.92	32.68	31.60	33.89	32.38	29.80
Noiseless	34.74	23.47	29.35	31.44	32.70	31.64	33.99	32.38	29.86
	Mandrill								
5	23.41	19.35	19.76	21.31	16.27	20.22	20.41	21.45	20.55
10	23.39	19.74	20.01	21.29	16.35	20.94	21.33	21.60	20.62
15	23.41	20.20	20.69	21.31	17.07	21.77	22.01	21.76	20.62
25	23.42	20.67	21.27	21.33	17.67	21.90	22.48	21.80	20.62
35	23.42	20.99	22.03	20.81	18.21	21.93	22.60	21.84	20.63
Noiseless	23.43	21.17	22.25	21.09	19.22	21.93	22.78	21.89	20.69
	Goldhill								
5	32.04	21.09	24.81	28.36	28.54	28.02	28.77	31.27	29.79
10	32.07	21.86	25.03	28.37	28.84	28.43	29.03	31.30	29.81
15	32.10	22.44	25.84	28.37	28.96	28.89	30.48	31.44	29.81
25	32.06	23.50	26.40	28.37	29.70	28.92	30.33	31.59	29.81
35	32.06	23.61	26.66	28.37	29.75	28.92	30.67	31.60	29.81
Noiseless	32.10	23.93	26.90	28.95	29.86	28.92	30.84	31.60	29.86
	Cameraman								
5	41.20	21.01	31.13	30.07	33.02	29.17	36.77	34.98	31.57
10	41.40	21.27	31.36	30.19	33.21	29.83	36.98	35.20	31.62
15	41.48	22.11	32.07	30.06	33.42	30.53	37.40	35.26	31.63
25	41.49	22.98	33.24	30.09	33.44	30.47	37.37	35.29	31.64
35	41.49	23.67	33.86	30.20	33.95	30.64	37.44	35.29	31.64
Noiseless	41.49	24.11	33.95	30.07	34.12	30.67	37.49	35.29	31.66
	Boat								
5	32.39	20.15	25.46	27.00	27.65	27.14	28.83	28.67	27.29
10	32.44	20.44	25.63	27.01	27.78	27.45	28.97	28.75	27.32
15	32.44	21.21	26.29	27.02	28.08	27.93	29.25	28.97	27.32
25	32.44	21.99	26.99	27.02	28.21	28.02	29.76	29.05	27.32
35	32.44	22.78	27.68	27.02	28.57	28.00	30.49	29.05	27.34
Noiseless	32.48	23.18	27.97	27.02	28.94	28.02	30.66	29.07	27.38

outperforms the other methods in all the cases, with PSNR improvements of up to 11.38dB and 13.68dB, as compared with BCS-SPL and TVAL3, respectively. Furthermore, the average PSNR gain by NLDR over BCS-SPL is 6.18dB and 5.17dB over TVAL3. For the other nonlocal based methods, we see that NLDR also outperforms them, with average PSNR gain over NLCS by 2.19dB, 5.41dB over TVNLR, 2.79Db over NLR-CS and 4.28dB over NLTV.

Since originally NLDR is calculated on top of the IST recovery algorithm with an extra nonlocal estimation step, in order to perform a fair comparison among the BCS-SPL and TVAL3 algorithms, we use the result image from BCS-SPL and TVAL3 algorithm as the input to the NLDR algorithm. By doing this, we would be able to quantify how much improvement NLDR has gained. Also, since the initial image from IST output is noisy, we further apply the state-of-the-art denoising algorithm - BM3D on top of the IST recovery result to denoise the result image in order to compare with the NLDR result.

In Table I, the column TVAL3+NLDR denotes applying NLDR on the TVAL3 resulting image, the column BCS-SPL+NLDR denotes NLDR applied on top of the BCS-SPL output, and IST+BM3D denotes BM3D applied on top of the IST output. Note, we also generate the sole IST algorithm output in the first column. From the table, we can see that the columns correspond to TVAL3+NLDR, BCS-SPL+NLDR and NLDR yield similar PSNR. This result indicates the generalization capability of NLDR, that it actually gives the best available denoised recovery result no matter what the initial input is. That is, NLDR has the great potential of serving as a stand-alone denoising algorithm.

Some visual results of CS reconstructed image *Barbara* with 30% measurement ratio are presented in Fig. 3. Obviously, NLDR generates much better visual quality than those from BCS-SPL and TVAL3, where both BCS-SPL and TVAL3 have blurred artifacts. When compared using Table I, we see NLDR outperforms the other two algorithms largely in PSNR. The reason is that the image *Barbara* itself has a lot of texture patterns (i.e., nonlocal similar patches), which had been successfully exploited in the NLDR algorithm. Fig. 4 demonstrates the *Boat* image with cropped character patch using 20% measurements. Also, we show in Fig. 5 the result of original NLDR using IST as well as TVAL3+NLDR and BCS-SPL+NLDR. They all have similar visual results as compared to the original image. This is consistent to the observation made based on Table I that their recovery PSNRs are very close.

2) Noisy Recovery: In this experiment, the robustness of the NLDR algorithm to noise is demonstrated. In practice, CS measurements consist mostly of linear operations, thus the Gaussian noise corrupting the signal during the signal acquisition is approximated as the Gaussian noise corrupting the compressed measurement vector. In our experiments, we simply corrupt the compressed measurement vector by different levels of Gaussian noise measured by Signal-to-Noise Ratios (SNRs). We use all seven standard test images and add different SNRs (5, 10, 15, 25, 35) to their 20% CS measurements and report the PSNR values of the final CS recovered image in Table II.

From Table II, we see that by adding 5dB of Gaussian noise on the CS measurements, all the TV-based algorithms' (i.e., TV, NLTV, TVAL3 and TVNLR) recovery performance suffer in terms of PSNR as compared with their original noiseless recovery settings. When the noise SNR reaches 35, the recovery result is close to its noiseless case. It also demonstrates that the recovery performance degrades on both BCS-SPL and NLCS when noise is added while NLDR is affected much less by the noise in all SNR cases. We see that the NLR-CS algorithm is also robust on noise with only less than 1dB PSNR decrease as compared with its noiseless settings for all the testing images. For BM3D, as a denoising algorithm, we see that the recovery result is not affected much with different noise dB levels. However, NLDR still outperforms NLR-CS and BM3D in the noisy CS recovery case.

B. Recovery Performance on MRI Data

In this experiment, the performance of the proposed NLDR algorithm is demonstrated on the real MRI Brain image data with a variety of undersampling factors. The image used is *in vivo* MR scans of size 512×512 from [31]. The CS data acquisition is simulated by downsampling the 2D discrete Fourier transform of the Brain image. Our result is

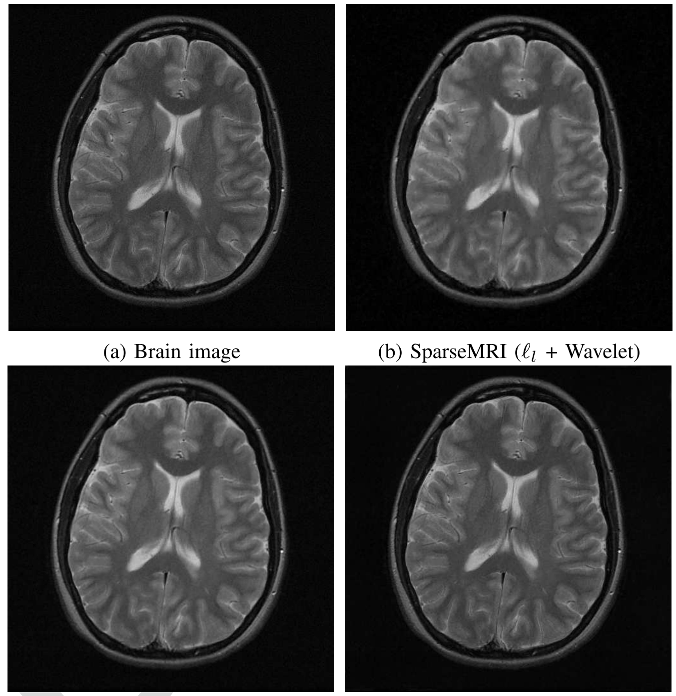

(a) Brain image (b) SparseMRI (ℓ_l + Wavelet)

(c) DLMRI (d) IST + NLDR

Fig. 6. Axial T2 Weighted Brain image CS recovery using 4 fold downsampling (25% measurements). (a) Original image; (b) reconstruction using SparseMRI, PSNR = 31.84dB; (c) DLMRI, PSNR = 34.75dB; (d) NLDR (IST), PSNR = 34.86dB.

compared with a leading CS MRI method by Lustig et al. [3] (denoted as SparseMRI) and the dictionary learning based recovery algorithm called DLMRI [32]. The SparseMRI method is to minimize both the l_1 norm and the TV norm of the image in the wavelet domain. The DLMRI uses K-SVD dictionary learning methods and tries to find the best sparse representation of the image for CS recovery. We adopt the same 2D random sampling scheme as in [32] with $2.5, 4, 6, 8, 10, 20$ fold downsampling. Here, for the k fold downsampling, it is equivalent to the measurement ratio (i.e., $\frac{m}{n}$) of $\frac{1}{k}$.

In Fig. 6, we present the CS recovery result on the Brain image with 4 fold downsampling. We observe that NLDR (based on IST) gives the best recovery result in PSNR which is 34.86dB. The DLMRI method also has a close PSNR of 34.75dB. We also demonstrate in Fig. 7 the comparison with various downsampling factors. When the downsampling factor is within 10 fold, the NLDR performance is comparable to that of the DLMRI method, while the SparseMRI generates much lower recovery PSNRs. When the downsampling factor reaches 20, the reconstructed image PSNR drops drastically for SparseMRI, and the NLDR is 1.15dB less than DLMRI PSNR. The reason that DLMRI performs better than NLDR is that, DLMRI uses dictionary learning to find the best sparse representation basis for each single test image. NLDR naturally utilizes a general DCT basis to represent the original test image. As a universal basis, it is not chosen to be optimal for one image. The DLMRI also has its disadvantages-the recovery time usually lasts for hours for a large image

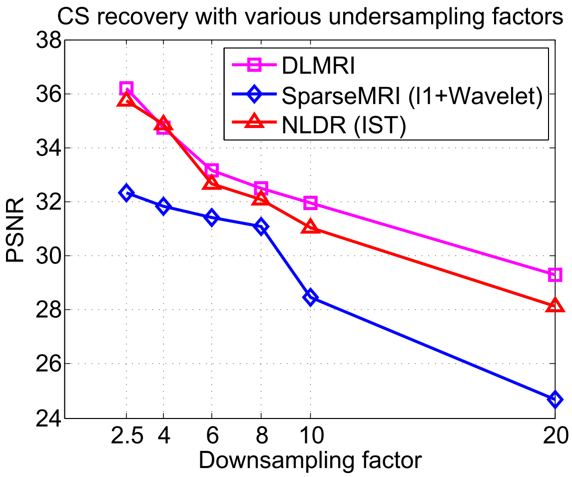

Fig. 7. CS recovery results comparison with various downsampling factors.

as the dictionary learning takes a lot of computations. The computation time needed for NLDR is at the same level as those of TVAL3 and BCS-SPL. For all our test images of size 512×512, NLDR takes, on average, about 10 minutes to finish on a Laptop PC.

V. Conclusion

This paper presented a CS image recovery algorithm based on Douglas-Rachford Splitting with nonlocal estimation. The proposed **NLDR** algorithm first used the iterative thesholding algorithm to obtain the intermediate image reconstruction result. Then a nonlocal estimation step was applied to the reconstructed image to improve the recovery performance. In the nonlocal estimation step, we reformulated the patches estimation as patch denoising problem using low-rank matrix approximation. We proposed a Douglas-Rachford splitting method to solve the CS recovery problem with the nonlocal estimation. Experimental results validated the performance of the proposed NLDR algorithm in both PSNR and visual perception on standard test images with both noiseless and noisy settings. NLDR outperformed the state-of-the-art CS recovery algorithms and showed it can be applied on top of existing recovery algorithms to further improve the recovery performance. Experiments on MRI data also demonstrated it is practical for real applications with competing results.

References

[1] D. L. Donoho, "Compressed sensing," *IEEE Trans. Inf. Theory*, vol. 52, no. 4, pp. 1289–1306, Apr. 2006.

[2] E. J. Candès, J. Romberg, and T. Tao, "Robust uncertainty principles: Exact signal reconstruction from highly incomplete frequency information," *IEEE Trans. Inf. Theory*, vol. 52, no. 2, pp. 489–509, Feb. 2006.

[3] M. Lustig, D. Donoho, and J. M. Pauly, "Sparse MRI: The application of compressed sensing for rapid MR imaging," *Magn. Reson. Med.*, vol. 58, no. 6, pp. 1182–1195, Dec. 2007.

[4] S. Mun and J. E. Fowler, "Block compressed sensing of images using directional transforms," in *Proc. 16th IEEE Int. Conf. Image Process. (ICIP)*, Nov. 2009, pp. 3021–3024.

[5] J. Zhang, D. Zhao, C. Zhao, R. Xiong, S. Ma, and W. Gao, "Compressed sensing recovery via collaborative sparsity," in *Proc. Data Compress. Conf. (DCC)*, Apr. 2012, pp. 287–296.

[6] C. Li, W. Yin, and Y. Zhang. (2009). *TVAL3: TV Minimization by Augmented Lagrangian and Alternating Direction Algorithms*. [Online]. Available: http://www.caam.rice.edu/~optimization/L1/TVAL3/

[7] L. Gan, "Block compressed sensing of natural images," in *Proc. 15th Int. Conf. Digit. Signal Process.*, Jul. 2007, pp. 403–406.

[8] J. Dahl, P. C. Hansen, S. H. Jensen, and T. L. Jensen, "Algorithms and software for total variation image reconstruction via first-order methods," *Numer. Algorithms*, vol. 53, no. 1, pp. 67–92, Jan. 2010.

[9] C. Louchet and L. Moisan, "Total variation as a local filter," *SIAM J. Imag. Sci.*, vol. 4, no. 2, pp. 651–694, 2011.

[10] M. Elad and M. Aharon, "Image denoising via sparse and redundant representations over learned dictionaries," *IEEE Trans. Image Process.*, vol. 15, no. 12, pp. 3736–3745, Dec. 2006.

[11] I. Daubechies, M. Defrise, and C. De Mol, "An iterative thresholding algorithm for linear inverse problems with a sparsity constraint," *Commun. Pure Appl. Math.*, vol. 57, no. 11, pp. 1413–1457, 2004.

[12] I. Daubechies, M. Fornasier, and I. Loris, "Accelerated projected gradient method for linear inverse problems with sparsity constraints," *J. Fourier Anal. Appl.*, vol. 14, nos. 5–6, pp. 764–792, 2008.

[13] A. Buades, B. Coll, and J. M. Morel, "A review of image denoising algorithms, with a new one," *Multiscale Model. Simul.*, vol. 4, no. 2, pp. 490–530, 2005.

[14] G. Peyré, S. Bougleux, and L. Cohen, "Non-local regularization of inverse problems," in *Computer Vision—ECCV*. Berlin, Germany: Springer-Verlag, 2008, pp. 57–68.

[15] Z. Yang and M. Jacob, "Nonlocal regularization of inverse problems: A unified variational framework," *IEEE Trans. Image Process.*, vol. 22, no. 8, pp. 3192–3203, Aug. 2013.

[16] J. Zhang, S. Liu, D. Zhao, R. Xiong, and S. Ma. (2012). "Improved total variation based image compressive sensing recovery by nonlocal regularization." [Online]. Available: http://arxiv.org/abs/1208.3716

[17] X. Shu, J. Yang, and N. Ahuja, "Non-local compressive sampling recovery," in *Proc. IEEE Int. Conf. Comput. Photography (ICCP)*, May 2014, pp. 1–8.

[18] W. Dong, G. Shi, X. Li, Y. Ma, and F. Huang, "Compressive sensing via nonlocal low-rank regularization," *IEEE Trans. Image Process.*, vol. 23, no. 8, pp. 3618–3632, Aug. 2014. AQ:3

[19] G. Chierchia, N. Pustelnik, B. Pesquet-Popescu, and J.-C. Pesquet, "A nonlocal structure tensor-based approach for multicomponent image recovery problems," *IEEE Trans. Image Process.*, vol. 23, no. 12, pp. 5531–5544, Dec. 2014.

[20] X. Zhang, M. Burger, X. Bresson, and S. Osher, "Bregmanized nonlocal regularization for deconvolution and sparse reconstruction," *SIAM J. Imag. Sci.*, vol. 3, no. 3, pp. 253–276, 2010.

[21] S. Osher, M. Burger, D. Goldfarb, J. Xu, and W. Yin, "An iterative regularization method for total variation-based image restoration," *Multiscale Model. Simul.*, vol. 4, no. 2, pp. 460–489, 2005.

[22] E. J. Candès and T. Tao, "The power of convex relaxation: Near-optimal matrix completion," *IEEE Trans. Inf. Theory*, vol. 56, no. 5, pp. 2053–2080, May 2010.

[23] W. Dong, G. Shi, and X. Li, "Nonlocal image restoration with bilateral variance estimation: A low-rank approach," *IEEE Trans. Image Process.*, vol. 22, no. 2, pp. 700–711, Feb. 2013.

[24] H. Ji, C. Liu, Z. Shen, and Y. Xu, "Robust video denoising using low rank matrix completion," in *Proc. IEEE Conf. Comput. Vis. Pattern Recognit. (CVPR)*, Jun. 2010, pp. 1791–1798.

[25] J. Douglas and H. Rachford, "On the numerical solution of heat conduction problems in two and three space variables," *Trans. Amer. Math. Soc.*, vol. 82, no. 2, pp. 421–439, 1956.

[26] P. L. Combettes and J.-C. Pesquet, "Proximal splitting methods in signal processing," in *Fixed-Point Algorithms for Inverse Problems in Science and Engineering*. Berlin, Germany: Springer-Verlag, 2011, pp. 185–212.

[27] P. L. Combettes and V. R. Wajs, "Signal recovery by proximal forward-backward splitting," *Multiscale Model. Simul.*, vol. 4, no. 4, pp. 1168–1200, 2005.

[28] *Software ℓ_1-Magic*. [Online]. Available: http://users.ece.gatech.edu/~justin/l1magic/, accessed Aug. 23, 2014.

[29] J. Zhang, S. Liu, R. Xiong, S. Ma, and D. Zhao, "Improved total variation based image compressive sensing recovery by nonlocal regularization," in *Proc. IEEE Int. Symp. Circuits Syst. (ISCAS)*, May 2013, pp. 2836–2839.

[30] K. Dabov, A. Foi, V. Katkovnik, and K. Egiazarian, "Image denoising by sparse 3D transform-domain collaborative filtering," *IEEE Trans. Image Process.*, vol. 16, no. 8, pp. 2080–2095, Aug. 2007.

[31] (2009). *American Radiology Services*. [Online]. Available: http://www3.americanradiology.com/pls/web1/wwimggal.vmg

[32] S. Ravishankar and Y. Bresler, "MR image reconstruction from highly undersampled k-space data by dictionary learning," *IEEE Trans. Med. Imag.*, vol. 30, no. 5, pp. 1028–1041, May 2011.

Shuangjiang Li received the B.S. degree in electrical engineering from the University of Science and Technology Beijing, Beijing, China, in 2009, and the M.S. and Ph.D. degrees in computer engineering from the University of Tennessee, Knoxville, TN, in 2011 and 2015, respectively. His research interests include signal and image processing, compressed sensing, mobile sensing systems, and WSN.

Hairong Qi (S'97–M'00–SM'05) received the B.S. and M.S. degrees in computer science from Northern JiaoTong University, Beijing, China, in 1992 and 1995, respectively, and the Ph.D. degree in computer engineering from North Carolina State University, Raleigh, in 1999.

She is currently the Gonzalez Family Professor with the Department of Electrical Engineering and Computer Science, University of Tennessee, Knoxville. Her current research interests are in advanced imaging and collaborative processing in resource-constrained distributed environment, hyperspectral image analysis, and automatic target recognition.

Dr. Qi was a recipient of the NSF CAREER Award. She also received the Best Paper Awards at the 18th International Conference on Pattern Recognition in 2006, the third ACM/IEEE International Conference on Distributed Smart Cameras in 2009, and the Seventh IEEE Workshop on Hyperspectral Image and Signal Processing: Evolution in Remote Sensor in 2015. She received the Highest Impact Paper from the IEEE Geoscience and Remote Sensing Society in 2012.

AUTHOR QUERIES

AQ:1 = Please confirm whether the corresponding author information is correct as set.
AQ:2 = Please note that some figures and tables are placed before their first citations in order to avoid having figures appear in the conclusion and references sections, which would be against IEEE style. Please confirm that the placement of all figures and tables are fine.
AQ:3 = Please note that references [18] and [20] are the same. Hence we deleted Ref. [20] and renumbered the other references. This change will also reflect in the citations present in the body text. Please confirm.

A Douglas–Rachford Splitting Approach to Compressed Sensing Image Recovery Using Low-Rank Regularization

Shuangjiang Li, *Student Member, IEEE*, and Hairong Qi, *Senior Member, IEEE*

***Abstract*— In this paper, we study the compressed sensing (CS) image recovery problem. The traditional method divides the image into blocks and treats each block as an independent sub-CS recovery task. This often results in losing global structure of an image. In order to improve the CS recovery result, we propose a nonlocal (NL) estimation step after the initial CS recovery for denoising purpose. The NL estimation is based on the well-known NL means filtering that takes an advantage of self-similarity in images. We formulate the NL estimation as the low-rank matrix approximation problem, where the low-rank matrix is formed by the NL similarity patches. An efficient algorithm, nonlocal Douglas–Rachford (NLDR), based on Douglas–Rachford splitting is developed to solve this low-rank optimization problem constrained by the CS measurements. Experimental results demonstrate that the proposed NLDR algorithm achieves significant performance improvements over the state-of-the-art in CS image recovery.**

***Index Terms*— Compressed sensing, image recovery, nonlocal filtering, Douglas-Rachford splitting, low-rank estimation.**

I. Introduction

COMPRESSED Sensing (CS) has drawn quite some attention as a joint sampling and compression approach [1], [2]. It states that under certain conditions, signals of interest can be sampled at a rate much lower than the Nyquist rate while still enabling exact reconstruction of the original signal. CS-based approach has an attractive advantage that the encoding process is made signal-independent and computationally inexpensive at the cost of high decoding/recovery complexity. Usually, the CS measurement is acquired through projecting the raw signals on to a pre-defined random sampling operator. Thus, CS is especially desirable in some image processing applications when the data acquisition devices must be simple (e.g., inexpensive resource-deprived sensors), or when oversampling can harm the object being captured (e.g., X-ray imaging) [3], among which the compressive sensing Magnetic Resonance Imaging (CS-MRI) is most promising as it significantly reduces the acquisition time of MRI scanning. When applied to 2D images, CS faces several challenges including a computationally expensive reconstruction process and huge memory required to store the random sampling operator [4]. Several fast algorithms have been developed for CS reconstruction [4]–[6]. The memory challenge was first addressed in [7] using a block-based sampling operation, which later on became the most common method in CS image recovery.

Block-based compressed sensing (BCS) has made the CS image recovery practical since it reduces the recovery cost, where image acquisition is conducted in a block-by-block manner through the same compressed sensing (CS) measurement operator. However, manually dividing the image into blocks and treating each image block as an independent sub-CS recovery task would inevitably lose some global properties of the image. Thus it would often require some filtering technique (i.e., Wiener filter [4]) to generate good visual recovery result. Nonetheless, the recovered image still suffers a low PSNR. Aside from BCS, another class of popular methods is based on the total variation (TV) model [5], [8], which exploits the prior knowledge that a natural image is sparse in the gradient domain. TV based algorithms often suffer from undesirable staircase artifacts and tend to over-smooth image details and textures [9].

In this paper, we propose **NLDR**, a CS image recovery algorithm based on the BCS scheme. We overcome the aforementioned BCS problems by introducing a new nonlocal estimation step after the initial CS reconstruction to further remove noise. The nonlocal estimation process is built on the well-known nonlocal means (NL) filtering that takes advantage of self-similarities in images, which preserves certain global structure. We formulate the nonlocal estimation into the low-rank approximation problem where the low-rank matrix is formed by the nonlocal similarity patches. Furthermore, by using a deterministic annealing (DA) approach, we incorporate the CS measurement constraint into the low-rank optimization problem. We propose an efficient algorithm based on Douglas-Rachford splitting (DR) to solve the low-rank matrix approximation problem combined with the CS measurement constraints, the solution to which is the final CS recovery output. The proposed NLDR algorithm effectively reduces the staircase artifacts that introduced in BCS and TV by utilizing the nonlocal similarity patches while preventing over-smoothness by recursively incorporating the initial CS measurement constraint.

Manuscript received December 28, 2014; revised May 20, 2015; accepted July 16, 2015. The associate editor coordinating the review of this manuscript and approving it for publication was Dr. Quanzheng Li. *(Corresponding author: Shuangjiang Li.)* AQ:1

The authors are with the Department of Electrical Engineering and Computer Science, University of Tennessee, Knoxville, TN 37996 USA (e-mail: sli22@vols.utk.edu; hqi@utk.edu).

Color versions of one or more of the figures in this paper are available online at http://ieeexplore.ieee.org.

Digital Object Identifier 10.1109/TIP.2015.2459653

The rest of the paper is organized as follows. Section II provides a brief review of the CS image recovery problem as well as some related works. Section III discusses the nonlocal estimation and Douglas-Rachford Splitting method. We conduct experiments in Section IV on both standard test images and MRI images. Section V concludes the paper.

II. Background and Related Works

A. CS Image Recovery Problem

Mathematically, the sparse representation model assumes that a signal $x \in \mathcal{R}^n$ can be represented as $x = \Psi\alpha$, where $\Psi \in \mathcal{R}^{n\times n}$ is a sparsifying basis or dictionary, and most entries of the coding vector α are zero or close to zero. This sparse decomposition of x can be obtained by solving a relaxed convex ℓ_1-minimization problem in the following Lagrangian form:

$$\min_{\alpha}\{\|x - \Psi\alpha\|_2^2 + \lambda_\alpha\|\alpha\|_1\}, \tag{1}$$

where constant λ_α denotes the regularization parameter.

In CS image recovery, we consider an image $I \in \mathcal{R}^{\sqrt{n}\times\sqrt{n}}$. By representing the image I in vector format, denoted as x, what we observe is the projected measurement y via $y = \Phi x + \nu$, where $\Phi \in \mathcal{R}^{m\times n}(m < n)$ is the measurement operator and ν is the additive noise vector. To recover x from y, first y is sparsely coded with respect to the basis Ψ by solving the following minimization problem

$$\hat{\alpha} = \arg\min_{\alpha}\{\|y - \Phi\Psi\alpha\|_2^2 + \lambda_\alpha\|\alpha\|_1\} \tag{2}$$

and then x is reconstructed by $\hat{x} = \Psi\hat{\alpha}$.

This can be easily extended to the block-based scenario, as stated in [10]. Let $x_i = R_i x$ denote an image patch extracted at location i, where R_i is the matrix extracting patch x_i from x at pixel location i. Given a basis Ψ, each patch can be sparse represented and solved by Eq. (1). Then the entire image x can be represented by the set of sparse code using $\{\Psi\alpha_i\}$. The patches can be overlapped to suppress the boundary artifacts.

Similarly, in order to reconstruct the image x from the measurement y, we can adopt the same block-based CS recovery by solving α_i from Eq. (2). The whole image x is then reconstructed as $\hat{x} = \Psi\hat{\alpha} = (\sum_i^N R_i^T R_i)^{-1}\sum_i^N(R_i^T\Phi\hat{\alpha}_i)$ as proved in [10].

The Iterative soft thresholding (IST) algorithm [11] can be very efficient in solving the problem in Eq. (2). In the $(k+1)$-th iteration, the solution is given by $\alpha^{(k+1)} = \mathcal{S}_\tau(\alpha^{(k)} + \Phi^* y - \Phi^*\Phi\Psi\alpha^{(k)})$, where $\mathcal{S}_\tau(\cdot)$ is the classic soft-thresholding operator [11]. In this paper, we use a slightly modified IST algorithm [12], where the solution in each iteration is called the *projected Landweber iteration* with the adaptive descent parameter $\beta^{(k)} > 0$,

$$\alpha^{(k+1)} = \mathcal{P}_{\mathcal{R}}[\alpha^{(k)} + \beta^{(k)}\Phi^*(y - \Phi\Psi\alpha^{(k)})], \tag{3}$$

where $\mathcal{P}_{\mathcal{R}}$ is the ℓ_2 projection of α on the ℓ_1 ball with radius $\mathcal{R}$. The adaptive descent parameter $\beta^{(k)}$ can be selected using the greedy strategy as follows,

$$\beta^{(k)} = \frac{\|\Phi^*(y - \Phi\Psi\alpha^{(k)})\|_2^2}{\|\Phi\Phi^*(y - \Phi\Psi\alpha^{(k)})\|_2^2} \tag{4}$$

This is an accelerated version of IST that converges faster than the original IST. Readers may refer to [12] for details.

B. Other Related Works

Buades et al. introduced in [13] the *nonlocal means* (NLM) filtering approach to image denoising, where the self-similarities between rectangular patches are used as a prior on natural images. The idea of nonlocal means has recently received much attention in image processing [14]–[19]. For example, Peyré et al. [14] proposed to use the Total Variation (TV) prior and nonlocal graph to solve the inverse problem with application in CS. The same idea was also adopted in Yang and Jacob [15]. Zhang et al. [16] proposed TVNLR which improves the conventional TV approach by adding a nonlocal regularization to the CS recovery problem and solved the problem using the Augmented Lagrangian Method (ALM). Shu et al. proposed the NLCS algorithm [17] and tried to group similar patches through NLS (nonlocal sparsity) regularization. The authors in [19] proposed a nonlocal total variation structure tensor (ST-NLTV) regularization approach for multicomponent image recovery from degraded observations, leading to significant improvements in terms of convergence speed over state-of-the-art methods such as the Alternating Direction Method of Multipliers (ADMM). Dong et al. proposed the nonlocal low-rank regularization (NLR-CS) method [18] which explored the structured sparsity of the image patches for compressed sensing. In order to explore the low-rank structure of the image patches, a smooth but non-convex surrogate function for the rank estimation is adopted as objective function. Zhang et al. proposed nonlocal TV regularization (NLVT) [20] for CS image recovery. NLTV is based on the Bregman iteration [21], namely Bregmanized Operator splitting (BOS).

In this paper, we adopt the nonlocal means filtering idea and introduce a new nonlocal estimation step after the initial CS reconstruction to further remove noise. It differs from [14] as we use the ℓ_1-norm based sparsity of the image and result in solving a convex optimization problem using the projection method. In [14] the nonlocal graph is similar to the nonlocal weights between patches as used in our paper. The main difference is that the author further imposed that these weights correspond to a probability distribution and that the graph only connects pixels that are not too far away. While in [15], the nonlocal weights may be improved using a different distance metric (i.e., robust distance metric) to promote the averaging of similar patches while minimizing the averaging of dissimilar patches. In this paper, we only aim to find similar patches to form low-rank matrix and thus differ from these methods. In [18] instead of using the nuclear norm for low-rank approximation, the authors proposed to use non-convex surrogate function and subsequently solved the optimization problem via ADMM.

In [17], two non-local sparsity measures, i.e., non-local wavelet sparsity and non-local joint sparsity, were proposed to exploit the patch correlation in NLCS. It then combines with the conventional TV measure to form the optimization objective function and use the ADMM method to solve the CS recovery problem. It differs from our algorithm in that their search for similar patches is incorporated in the objective function while NLDR directly adopts the nonlocal means filtering approach to find the similar patches and then conducts low-rank approximation. After getting the non-local low-rank estimation, we further incorporate the initial CS measurement constraint into the low-rank optimization problem, using a deterministic annealing (DA) approach to further improve the recovery result. Additionally, compared to the traditional ADMM method, we propose to use Douglas-Rachford splitting method to effectively solve the combined optimization problem.

In [22], Candès and Tao proposed to solve the matrix completion problem using low-rank regularization through convex optimization. Later in [23] Dong et al. first combined the nonlocal image representation and low-rank approach for image restoration and achived state-of-the-art performance in image denosing. Ji et al. [24] also incorporated the low-rank matrix completion in video denoising.

To summarize, the main contribution of this paper is three-fold: First, we propose to incorporate the nonlocal similarity patches searching step after the initial CS image recovery task. By searching and incorporating the nonlocal similarity patches the traditional block based CS recovery artifacts could be resolved. Second, we propose to estimate the grouped similarity patches matrix as a low-rank matrix completion problem, referred as nonlocal low-rank estimation. The idea is that, by searching the nonlocal similarity patches we could resolve the block and staircase artifacts, while using low-rank estimation we can further denoise the grouped similarity patches. Third, we incorporate the initial CS measurement constraint into the low-rank estimation optimization problem. By using a deterministic annealing (DA) approach, the Douglas-Rachford splitting effectively solves the reformulated optimization problem.

III. Nonlocal Low-Rank Regularization and Douglas-Rachford Splitting

In this section, we present the idea of nonlocal low-rank regularization, followed by the proposed Douglas-Rachford splitting method. We refer to the algorithm as the Nonlocal Douglas-Rachford splitting (NLDR) algorithm.

A. Nonlocal Low-Rank Regularization for CS Image

An example to illustrate the nonlocal estimation step is shown in Fig. 1. The *Lena* image in the first row is obtained from the IST CS recovery algorithm. Then the nonlocal similar patches are searched across the entire image. We denote the nonlocal similar patches of x_i as $x_{i,1}, x_{i,2}, x_{i,3}, \cdots x_{i,q}$. These extracted patches then form the matrix B_i where the low-rank approximation is conducted to yield the resulting denoised patch matrix, as shown in the second row. We apply patch reweight to obtain the estimated patch x_e to update the original patch x_i. After iterating over the entire image, the much cleaner *Lena* image is shown leftmost in the second row.

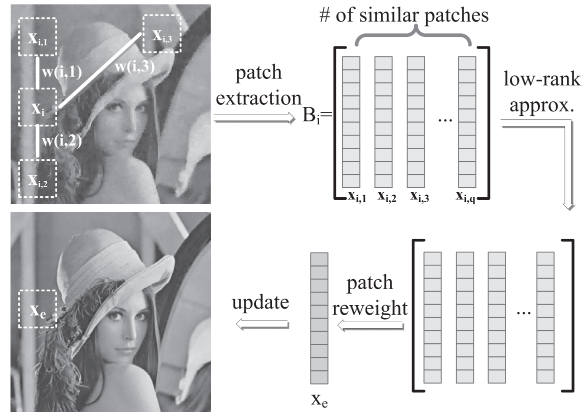

Fig. 1. An illustration of nonlocal estimation and similar patches denoising using low-rank matrix approximation.

1) *Nonlocal Similarity Patches:* The basic idea of nonlocal (NL) means filtering is simple. For a given pixel u_i in an image x, its NL filtered new intensity value, denoted by $NL(u_i)$, is obtained as a weighted average of its neighborhood pixels within a search window of size w.

In our work, we extend the pixel-wise nonlocal filtering to the patch-based filtering. Specifically, we search for the nonlocal similar "patches" $x_{i,j}$, $j = 1, 2, \cdots, q$, to the given patch x_i in a large window of size w centered at pixel u_i. Here, q is the total number of similar patches to be selected. The weight of patch $x_{i,j}$ to x_i, denoted as ω_{ij}, is then computed by

$$\omega_{ij} = \frac{1}{c_i}\exp\left(\frac{-\|x_i - x_{i,j}\|_2^2}{h^2}\right), \quad j = 1, \cdots, q \tag{5}$$

where h is a pre-determined scalar and c_i is the normalization factor. Accordingly, for each patch x_i, we have a set of its similar patches, denoted by $\boldsymbol{\Omega}_i$. Then the nonlocal estimates of each patch $\hat{x}_i$ can be computed as $\hat{x}_i = \sum_{j\in\Omega_i} \omega_{ij} x_{i,j}$. Further, this can be written in a matrix form as

$$\hat{x}_{nl} \doteq \mathbf{W}\sum_{i=1}^{p} \hat{x}_i, \quad \mathbf{W}(i,j) = \begin{cases} \omega_{ij}, & \text{if } x_j \in \Omega_i \\ 0, & \text{otherwise.} \end{cases} \tag{6}$$

where p denotes the number of all patches in the entire image and $\hat{x}_{nl}$ is the nonlocal estimated image output.

2) *Patch Denoising by Low-Rank Approximation:* Although we can use Eq. (6) to remove noise in the IST recovered image $\hat{x}$ to a certain degree, this is based on a weighted average of patches in $\hat{x}$, which are inherently noisy. Thus, it is imperative to apply some denoising techniques before the nonlocal similarity patch reweight using Eq. (6) to prevent the noise from accumulating. By rewriting the nonlocal similarity patches into the matrix format, we have $B_i = [x_{i,1}; x_{i,2}; , \cdots ; x_{i,q}]$, where each column of B_i is a vector representation of $x_{i,j}$, $j = 1, 2, \cdots, q$ for patch x_i. Since all columns of B_i share similarity with patch x_i, the columns of B_i should bear a high degree of similarity between each other. In other words, we can safely treat B_i as a low-rank matrix. We thus formulate the nonlocal patch denoising problem into the low-rank matrix approximation

problem [22] as follows,

$$\min_{\hat{B}_i} \frac{1}{2}\|B_i - \hat{B}_i\|_2^2 + \lambda_{B_i}\|\hat{B}_i\|_*, \tag{7}$$

where $\|\hat{B}_i\|_*$ is the nuclear norm of the low-rank approximated patch matrix $\hat{B}_i$, defined by $\|\hat{B}_i\|_* \triangleq \text{trace}(\sqrt{\hat{B}_i^T \hat{B}_i}) = \sum_{r=1}^{q} \sigma_r$, and σ_r's are the singular values of $\hat{B}_i$.

In addition, since the columns of B_i (or the patches) are also a subset of the reconstructed image from IST recovery algorithm, it should be subject to the CS measurement constraint $y = \Phi x$. Therefore, multiplying Eq. (7) with $\mathbf{W}$, we reformulate the denoising problem of Eq. (7) into

$$\min_{x} \frac{1}{2}\|x - \mathbf{W}B_i\|_2^2 + \lambda_x\|x\|_* \text{ s.t. } y = \Phi x. \tag{8}$$

In what follows, we discuss in sec. III-B how to solve Eq. (8) with the CS measurement constraint using the method referred to as the Douglas-Rachford splitting method.

B. Douglas-Rachford Splitting

The Douglas-Rachford splitting method was originally proposed in [25] for solving matrix equations. Later on it was advanced as an iterative scheme to minimize the functions of the form,

$$\min_{x} F(x) + G(x) \tag{9}$$

where both F and G are convex functions for which one is able to compute the proximal mappings $\mathsf{prox}_{\gamma F}$ and $\mathsf{prox}_{\gamma G}$ which are defined as

$$\mathsf{prox}_{\gamma F}(x) = \arg\min_{y} \frac{1}{2}\|x - y\|_2^2 + \gamma F(y) \tag{10}$$

The same definition applies to $\mathsf{prox}_{\gamma G}$ [26]. In order to solve Eq. (8), we have $F(x) = \iota_{\mathcal{C}}(x)$ and $G(x) = \|x\|_*$, where $\mathcal{C} = \{x : y = \Phi x\}$ and $\iota_{\mathcal{C}}$ is the indicator function.

Given that $F(x) = \iota_{\mathcal{C}}(x)$, the solution to Eq. (10) is the same as projections onto convex sets (POCS), and does not depend on γ. Therefore, we have

$$\mathsf{prox}_{\gamma \iota_{\mathcal{C}} F}(x) = \mathsf{prox}_{\iota_{\mathcal{C}} F}(x) = x + \Phi^+(y - \Phi x), \tag{11}$$

where $\Phi^+ = \Phi^T(\Phi\Phi^T)^{-1}$ is the pseudoinverse of Φ. The proximal operator of $G(x)$ is the soft thresholding of the singular values

$$\mathsf{prox}_{\gamma G}(x) = U(x) \cdot \rho_{\lambda_x}(S(x)) \cdot V(x)^* \tag{12}$$

where $x = U \cdot S \cdot V^*$ is the singular value decomposition of the matrix x and $S = \text{diag}(s_i)_i$ is the diagonal matrix of singular values s_i, and $\rho_{\lambda_x}(S)$ is defined as a diagonal operator.

$$\rho_\lambda(S) = \text{diag}(\max(0, 1 - \lambda_x/|s_i|)s_i)_i \tag{13}$$

We can then solve the problem in Eq. (7) using the Douglas-Rachford iterations given by

$$\tilde{x}_{k+1} = (1 - \frac{\mu}{2})\tilde{x}_k + \frac{\mu}{2}\mathsf{rprox}_{\gamma G}(\mathsf{rprox}_{\gamma F}(\tilde{x}_k)) \tag{14}$$

and the $(k+1)$-th solution $\hat{x}_{k+1}$ is calculated by $\hat{x}_{k+1} = \mathsf{prox}_{\gamma F}(\tilde{x}_{k+1})$. Here the reversed-proximal mappings is given by $\mathsf{rprox}_{\gamma F} = 2\mathsf{prox}_{\gamma F} - x$ for $F(x)$ and in the similar fashion to G(x).. The parameters are selected as $\lambda_x > 0$ and $0 < \mu < 2$ which guarantee $\hat{x}$ to be a solution that minimizes $F(x) + G(x)$ based on the proof in [27].

Algorithm 1 Nonlocal Douglas-Rachford Splitting (NLDR) Algorithm

---

Input:

- ▶ Measurement matrix $\Phi \in \mathbb{R}^{m \times n}$
- ▶ Basis matrix $\Psi \in \mathbb{R}^{n \times n}$
- ▶ Observation vector $y \in \mathbb{R}^m$.
- ▶ Number of IST iterations iter, number of nonlocal estimation iterations J, DR splitting iterations K

Output:

- ▶ An estimate $\hat{x} \in \mathbb{R}^n$ of the original image x.

```
Initialize α^0 ← 0
for k = 1, ··· , iter do
    (a) Select β^(k) based on Eq. (4)
    (b) Update α^(k+1) using Eq. (3)
end for
for j = 1, 2, ··· , J do
Step 1: Nonlocal Estimate
    (a) Calculate nonlocal weights ω_ij via Eq. (5)
    (b) Obtain low-rank patch matrix B_i via Eq. (7)
Step 2: Douglas-Rachford Splitting to solve Eq. (8)
    for k = 1, 2, ··· , K do
    (a) Calculate prox_γF(x) via Eq. (11)
    (b) Calculate prox_γG(x) via Eq. (12)
    (c) Calculate x̃_(k+1) via Eq. (14)
    end for
end for
return x̂ ← x̃_(k+1)
```

C. The NLDR Algorithm

Algorithm 1 provides a pseudo-code for the proposed Nonlocal Douglas-Rachford splitting (NLDR) algorithm. Given the observation y (i.e., compressed measurements), the NLDR algorithm first outputs an intermediate reconstruction result $\hat{x}_{IST}$ through the IST algorithm. This soft-thresholding output is then used to calculate the nonlocal estimated image $\hat{x}_{nl}$, which is used to initialize the low-rank optimization problem in Eq. (7) where the Douglas-Rachford splitting method will be carried out iteratively based on Eq. (14).

As for calculating the nonlocal estimates of the image, the NLDR algorithm obtains the averaged result based on J nonlocal estimation iterations. For the IST algorithm, we empirically set the penalty parameter $\lambda_\alpha = 1.8$ and soft-thresholding parameter $\tau = 1.2$, respectively.

IV. EXPERIMENTS

In this section, we evaluate the NLDR algorithm for CS image reconstruction where both standard test images and MRI images are used. The reason for choosing MRI images for evaluation purpose is due to the significant impact of CS on the clinical practice of MRI, where long acquisition time

TABLE I

PSNR PERFORMANCE IN dB

Images		Lena											
Algorithms		IST	TV	TVAL3	BCS-SPL	IST+BM3D	NLCS	TVNLR	NLR-CS	NLTV	NLDR	TVAL3+NLDR	BCS-SPL+NLDR
m/n	0.1	25.41	22.75	29.02	28.31	25.93	31.74	28.62	29.58	25.94	33.67	**33.81**	33.80
	0.2	29.57	24.44	31.56	31.37	30.42	34.78	30.98	32.95	29.73	36.33	**36.35**	**36.35**
	0.3	32.05	25.47	32.99	33.50	32.91	36.67	33.52	34.73	31.73	37.82	**37.83**	**37.83**
	0.4	34.07	27.88	35.03	35.20	34.72	38.22	35.48	36.56	35.39	**39.02**	**39.02**	**39.02**
	0.5	35.89	30.73	36.26	36.79	36.34	39.66	36.94	38.77	37.90	40.16	**40.17**	40.16
		Barbara											
m/n	0.1	21.18	20.10	21.31	22.85	21.34	24.34	22.55	26.90	23.13	29.48	**31.14**	31.01
	0.2	24.35	21.66	21.60	24.33	24.80	28.17	24.30	30.87	28.29	**35.28**	35.21	35.22
	0.3	26.96	23.61	24.79	25.92	27.73	31.65	25.35	34.26	31.79	37.30	37.30	**37.32**
	0.4	29.38	25.32	28.55	27.68	30.29	34.32	26.85	36.14	34.44	**38.95**	**38.95**	**38.95**
	0.5	31.73	26.62	31.08	30.15	32.82	36.63	28.02	39.36	36.23	40.50	**40.51**	**40.51**
		Peppers											
m/n	0.1	24.30	21.98	29.69	28.88	24.77	31.85	26.25	29.18	25.78	32.91	**33.11**	33.07
	0.2	29.16	23.47	32.70	31.44	29.86	33.99	31.64	32.38	29.35	**34.74**	34.70	34.69
	0.3	31.54	25.57	34.02	32.89	32.16	35.27	34.35	33.73	32.85	**35.78**	35.70	35.70
	0.4	33.29	27.56	34.98	34.06	33.57	36.41	35.62	35.29	34.82	**36.91**	36.75	36.75
	0.5	34.73	29.67	36.08	35.18	34.57	37.52	36.74	37.03	36.96	**38.13**	37.99	37.99
		Mandrill											
m/n	0.1	19.68	19.79	19.01	20.21	19.66	20.89	20.37	20.63	19.95	21.15	**21.89**	21.80
	0.2	21.02	21.17	19.22	21.09	20.69	22.78	21.93	21.89	22.25	23.43	**24.08**	23.93
	0.3	22.34	22.81	19.70	21.80	21.79	24.44	23.11	23.21	24.64	25.49	**25.85**	25.73
	0.4	23.68	24.79	20.20	22.92	23.13	26.17	24.26	25.20	26.95	27.47	**27.91**	27.81
	0.5	25.16	26.71	22.73	24.50	24.72	27.87	25.42	27.16	29.37	29.40	**29.71**	29.66
		Goldhill											
m/n	0.1	24.96	22.56	27.45	26.96	25.08	28.53	25.20	28.92	23.58	28.94	**29.66**	29.57
	0.2	27.81	23.93	29.86	28.95	27.87	30.84	28.92	31.60	26.90	32.10	**32.26**	32.24
	0.3	29.53	25.88	31.62	30.56	29.49	32.55	31.29	33.37	30.08	33.99	**34.02**	**34.02**
	0.4	31.23	27.73	33.21	32.09	30.92	34.13	33.08	34.36	32.66	35.61	**35.63**	35.62
	0.5	32.76	29.44	33.29	33.61	32.18	35.67	34.55	36.41	35.01	37.20	37.20	**37.21**
		Cameraman											
m/n	0.1	23.86	22.05	28.50	26.36	24.38	33.26	25.53	30.72	29.71	36.83	**36.97**	36.85
	0.2	26.97	24.11	34.12	30.07	31.66	37.49	30.67	35.29	33.95	41.49	**41.56**	41.55
	0.3	33.66	26.55	38.16	32.82	35.44	40.71	34.34	37.79	37.65	43.92	**43.96**	**43.96**
	0.4	34.85	29.23	40.42	35.48	38.28	43.40	37.56	41.65	40.83	45.96	**46.01**	45.95
	0.5	36.26	34.02	43.01	37.85	40.71	45.92	39.95	45.56	43.67	47.90	**47.92**	47.90
		Boat											
m/n	0.1	23.77	21.48	25.76	24.65	24.16	27.74	24.03	26.41	23.94	28.69	**29.52**	29.24
	0.2	27.01	23.18	28.94	27.02	27.38	30.66	28.02	29.07	27.97	32.48	**32.68**	32.63
	0.3	29.10	24.84	31.09	28.94	29.61	32.64	30.80	30.65	30.89	34.41	**34.47**	34.43
	0.4	30.91	26.93	32.68	30.59	31.24	34.26	33.06	32.48	33.45	35.77	35.81	**35.86**
	0.5	32.68	29.19	33.53	32.19	32.76	35.73	34.66	35.87	36.04	37.24	37.24	**37.25**

has been one of the primary obstacles. We implement the algorithm using *Matlab* 2013b on a 2.20GHz laptop computer. BCS-SPL [4] is a block-based CS image recovery method solved using a smoothed version of projected Landweber (SPL) algorithm. The smoothing process is done by the Wiener filter. We further compare our result with one of the state-of-the-art algorithms for image CS recovery, known as TVAL3 [6]. TVAL3 tries to minimize the image total variation norm using augmented lagrangian and alternating direction algorithms. Several TV-based methods are also compared. The TV benchmark method denoted as TV which is implemented based on [28], TVNLR [29] and NLTV [20]. We also compare NLDR performance with other nonlocal based approaches, e.g., NLCS [17] and NLR-CS [18]. Finally, to evaluate the potential of NLDR as a standalone denoising method, we compare its performance with the state-of-the-art BM3D [30] method for noise removal purpose.

A. CS Recovery on Standard Image Dataset

We present the experimental results for noiseless CS measurements and then report the results using noisy CS measurements.

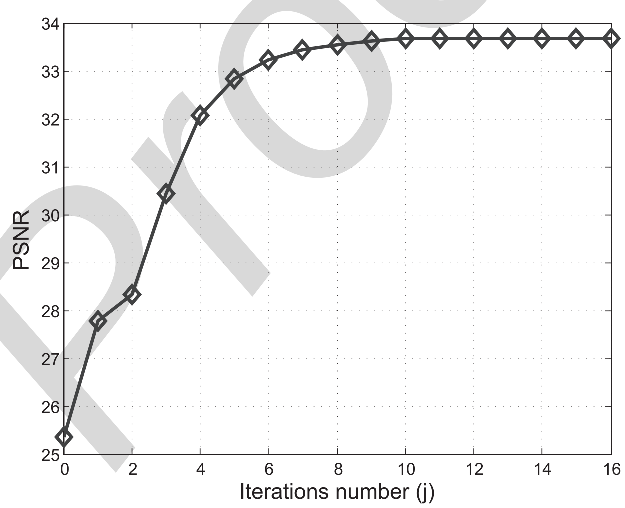

AQ:2

Fig. 2. CS recovery results on *Lena* image with 10% measurements at iteration j.

1) Noiseless Recovery: We first test the NLDR algorithm in noiseless settings using standard test images of size 512×512. The block-based image patch is of size 6×6. We set the number of similar patches q in the nonlocal

Fig. 3. CS Reconstructed image *Barbara* with 30% measurement ratio. (a) Original image; (b) proposed **NLDR** recovery, PSNR = 37.30dB; (c) BCS-SPL recovery [4], PSNR = 25.92dB; (d) TVAL3 recovery [6], PSNR = 24.79dB; (e) TVNLR recovery [29], PSNR = 25.35dB. (f) NLCS recovery [17], PSNR = 31.65dB; (g) NLR-CS recovery [18], PSNR = 34.26dB; (h) NLTV recovery [20], PSNR = 31.79dB.

Fig. 4. *Boat* image with cropped character patch using 20% measurements. (a) proposed **NLDR** recovery, PSNR = 32.48dB; (b) NLCS recovery [17], PSNR = 30.66dB; (c) TVNLR recovery [29], PSNR = 28.02dB; (d) NLR-CS recovery [18], PSNR = 29.07dB; (e) NLTV recovery [20], PSNR = 27.97dB.

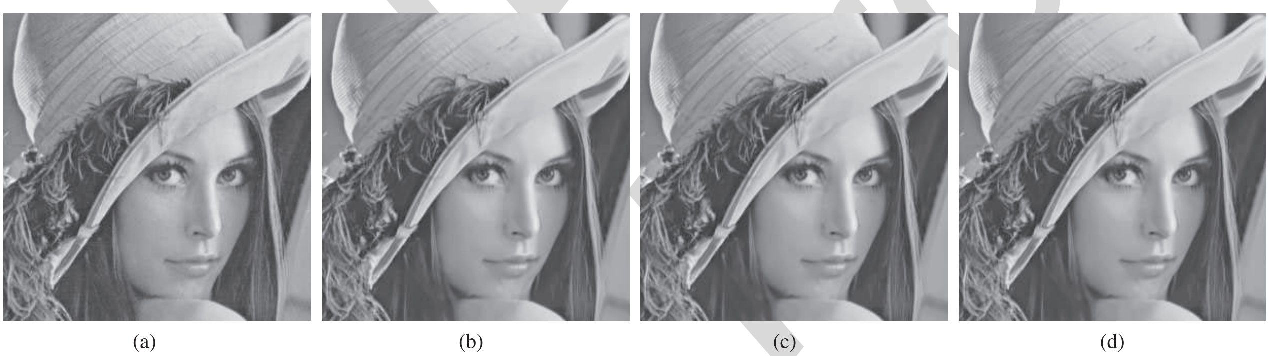

Fig. 5. Part of *Lena* image with 200% magnification using 20% measurements. (a) Original image; (b) reconstruction using proposed NLDR with IST, PSNR = 36.33dB; (c) TVAL3 + NLDR, PSNR = 36.35dB (d) BCS-SPL + NLDR, PSNR = 36.35dB.

estimation step as 45. We use the scrambled Fourier matrix as the CS measurement operator Φ and DCT matrix as the basis Ψ to represent the original image in the initial IST recovery. The parameters are selected as $\mu = 1$ for DR iteration and $\lambda_x = \frac{c_i}{\max(s_i)}$ for each iteration where $c_i = C_0 * \epsilon, 0 < \epsilon < 1$ and C_0 is a constant. For the number of iterations in the outerloop, we find that the recovery result gradually converges when J reaches 12 for all the image datasets. Fig. 2 shows one example on *Lena* image using 10% of measurements. Note that at iteration 0, we use the initial IST recovery result.

Table I compares PSNR with different measurement ratios (i.e., $\frac{m}{n}$). We see that the NLDR algorithm considerably

TABLE II
CS NOISY RECOVERY RESULTS ON STANDARD TEST IMAGES WITH 20% MEASUREMENTS

	Algorithm								
	NLDR	**TV**	**NLTV**	**BCS-SPL**	**TVAL3**	**TVNLR**	**NLCS**	**NRL-CS**	**BM3D**
SNR	**Lena**								
5	36.24	21.27	25.94	30.50	28.82	28.14	32.45	32.55	30.32
10	36.29	21.63	27.66	30.51	28.93	28.43	33.13	32.65	30.31
15	36.29	22.19	28.34	30.52	30.94	29.23	33.44	32.76	30.31
25	36.29	23.63	29.01	30.52	31.18	30.96	34.01	32.90	30.34
35	36.29	24.34	29.50	30.52	31.18	30.98	34.57	32.95	30.34
Noiseless	36.33	24.44	29.73	31.37	31.56	30.98	34.78	32.95	30.42
	Barbara								
5	35.15	19.03	25.11	24.40	19.45	23.22	27.73	30.39	24.74
10	35.16	19.34	25.94	24.44	19.80	23.56	27.86	30.50	24.75
15	35.16	19.87	26.37	24.45	19.94	24.17	28.02	30.76	24.77
25	35.21	21.05	27.35	24.45	20.03	24.04	27.94	30.87	24.77
35	35.27	21.32	28.04	24.46	20.07	24.28	28.01	30.87	24.80
Noiseless	35.28	21.66	28.29	24.33	21.60	24.30	28.17	30.87	24.80
	Peppers								
5	34.61	20.11	26.21	30.77	31.33	29.87	32.11	32.01	29.79
10	34.61	20.49	26.73	30.77	31.71	30.01	32.49	32.17	29.73
15	34.68	21.61	27.01	30.92	31.99	30.55	33.41	32.30	29.76
25	34.68	23.20	28.35	30.92	32.66	31.60	33.37	32.38	29.80
35	34.58	23.44	29.22	30.92	32.68	31.60	33.89	32.38	29.80
Noiseless	34.74	23.47	29.35	31.44	32.70	31.64	33.99	32.38	29.86
	Mandrill								
5	23.41	19.35	19.76	21.31	16.27	20.22	20.41	21.45	20.55
10	23.39	19.74	20.01	21.29	16.35	20.94	21.33	21.60	20.62
15	23.41	20.20	20.69	21.31	17.07	21.77	22.01	21.76	20.62
25	23.42	20.67	21.27	21.33	17.67	21.90	22.48	21.80	20.62
35	23.42	20.99	22.03	20.81	18.21	21.93	22.60	21.84	20.63
Noiseless	23.43	21.17	22.25	21.09	19.22	21.93	22.78	21.89	20.69
	Goldhill								
5	32.04	21.09	24.81	28.36	28.54	28.02	28.77	31.27	29.79
10	32.07	21.86	25.03	28.37	28.84	28.43	29.03	31.30	29.81
15	32.10	22.44	25.84	28.37	28.96	28.89	30.48	31.44	29.81
25	32.06	23.50	26.40	28.37	29.70	28.92	30.33	31.59	29.81
35	32.06	23.61	26.66	28.37	29.75	28.92	30.67	31.60	29.81
Noiseless	32.10	23.93	26.90	28.95	29.86	28.92	30.84	31.60	29.86
	Cameraman								
5	41.20	21.01	31.13	30.07	33.02	29.17	36.77	34.98	31.57
10	41.40	21.27	31.36	30.19	33.21	29.83	36.98	35.20	31.62
15	41.48	22.11	32.07	30.06	33.42	30.53	37.40	35.26	31.63
25	41.49	22.98	33.24	30.09	33.44	30.47	37.37	35.29	31.64
35	41.49	23.67	33.86	30.20	33.95	30.64	37.44	35.29	31.64
Noiseless	41.49	24.11	33.95	30.07	34.12	30.67	37.49	35.29	31.66
	Boat								
5	32.39	20.15	25.46	27.00	27.65	27.14	28.83	28.67	27.29
10	32.44	20.44	25.63	27.01	27.78	27.45	28.97	28.75	27.32
15	32.44	21.21	26.29	27.02	28.08	27.93	29.25	28.97	27.32
25	32.44	21.99	26.99	27.02	28.21	28.02	29.76	29.05	27.32
35	32.44	22.78	27.68	27.02	28.57	28.00	30.49	29.05	27.34
Noiseless	32.48	23.18	27.97	27.02	28.94	28.02	30.66	29.07	27.38

outperforms the other methods in all the cases, with PSNR improvements of up to 11.38dB and 13.68dB, as compared with BCS-SPL and TVAL3, respectively. Furthermore, the average PSNR gain by NLDR over BCS-SPL is 6.18dB and 5.17dB over TVAL3. For the other nonlocal based methods, we see that NLDR also outperforms them, with average PSNR gain over NLCS by 2.19dB, 5.41dB over TVNLR, 2.79Db over NLR-CS and 4.28dB over NLTV.

Since originally NLDR is calculated on top of the IST recovery algorithm with an extra nonlocal estimation step, in order to perform a fair comparison among the BCS-SPL and TVAL3 algorithms, we use the result image from BCS-SPL and TVAL3 algorithm as the input to the NLDR algorithm. By doing this, we would be able to quantify how much improvement NLDR has gained. Also, since the initial image from IST output is noisy, we further apply the state-of-the-art denoising algorithm - BM3D on top of the IST recovery result to denoise the result image in order to compare with the NLDR result.

In Table I, the column TVAL3+NLDR denotes applying NLDR on the TVAL3 resulting image, the column BCS-SPL+NLDR denotes NLDR applied on top of the BCS-SPL output, and IST+BM3D denotes BM3D applied on top of the IST output. Note, we also generate the sole IST algorithm output in the first column. From the table, we can see that the columns correspond to TVAL3+NLDR, BCS-SPL+NLDR and NLDR yield similar PSNR. This result indicates the generalization capability of NLDR, that it actually gives the best available denoised recovery result no matter what the initial input is. That is, NLDR has the great potential of serving as a stand-alone denoising algorithm.

Some visual results of CS reconstructed image *Barbara* with 30% measurement ratio are presented in Fig. 3. Obviously, NLDR generates much better visual quality than those from BCS-SPL and TVAL3, where both BCS-SPL and TVAL3 have blurred artifacts. When compared using Table I, we see NLDR outperforms the other two algorithms largely in PSNR. The reason is that the image *Barbara* itself has a lot of texture patterns (i.e., nonlocal similar patches), which had been successfully exploited in the NLDR algorithm. Fig. 4 demonstrates the *Boat* image with cropped character patch using 20% measurements. Also, we show in Fig. 5 the result of original NLDR using IST as well as TVAL3+NLDR and BCS-SPL+NLDR. They all have similar visual results as compared to the original image. This is consistent to the observation made based on Table I that their recovery PSNRs are very close.

2) Noisy Recovery: In this experiment, the robustness of the NLDR algorithm to noise is demonstrated. In practice, CS measurements consist mostly of linear operations, thus the Gaussian noise corrupting the signal during the signal acquisition is approximated as the Gaussian noise corrupting the compressed measurement vector. In our experiments, we simply corrupt the compressed measurement vector by different levels of Gaussian noise measured by Signal-to-Noise Ratios (SNRs). We use all seven standard test images and add different SNRs (5, 10, 15, 25, 35) to their 20% CS measurements and report the PSNR values of the final CS recovered image in Table II.

From Table II, we see that by adding 5dB of Gaussian noise on the CS measurements, all the TV-based algorithms' (i.e., TV, NLTV, TVAL3 and TVNLR) recovery performance suffer in terms of PSNR as compared with their original noiseless recovery settings. When the noise SNR reaches 35, the recovery result is close to its noiseless case. It also demonstrates that the recovery performance degrades on both BCS-SPL and NLCS when noise is added while NLDR is affected much less by the noise in all SNR cases. We see that the NLR-CS algorithm is also robust on noise with only less than 1dB PSNR decrease as compared with its noiseless settings for all the testing images. For BM3D, as a denoising algorithm, we see that the recovery result is not affected much with different noise dB levels. However, NLDR still outperforms NLR-CS and BM3D in the noisy CS recovery case.

B. Recovery Performance on MRI Data

In this experiment, the performance of the proposed NLDR algorithm is demonstrated on the real MRI Brain image data with a variety of undersampling factors. The image used is *in vivo* MR scans of size 512×512 from [31]. The CS data acquisition is simulated by downsampling the 2D discrete Fourier transform of the Brain image. Our result is compared with a leading CS MRI method by Lustig et al. [3] (denoted as SparseMRI) and the dictionary learning based recovery algorithm called DLMRI [32]. The SparseMRI method is to minimize both the l_1 norm and the TV norm of the image in the wavelet domain. The DLMRI uses K-SVD dictionary learning methods and tries to find the best sparse representation of the image for CS recovery. We adopt the same 2D random sampling scheme as in [32] with $2.5, 4, 6, 8, 10, 20$ fold downsampling. Here, for the k fold downsampling, it is equivalent to the measurement ratio (i.e., $\frac{m}{n}$) of $\frac{1}{k}$.

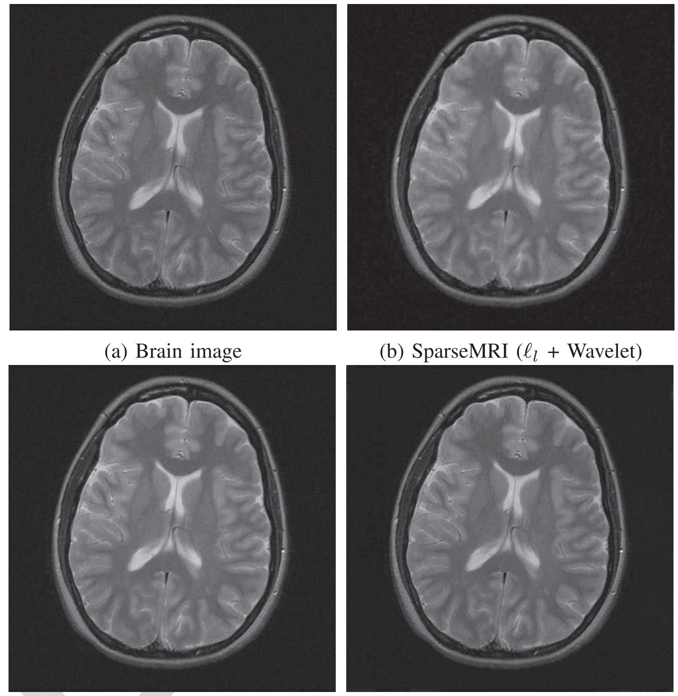

(a) Brain image (b) SparseMRI (ℓ_l + Wavelet) (c) DLMRI (d) IST + NLDR

Fig. 6. Axial T2 Weighted Brain image CS recovery using 4 fold downsampling (25% measurements). (a) Original image; (b) reconstruction using SparseMRI, PSNR = 31.84dB; (c) DLMRI, PSNR = 34.75dB; (d) NLDR (IST), PSNR = 34.86dB.

In Fig. 6, we present the CS recovery result on the Brain image with 4 fold downsampling. We observe that NLDR (based on IST) gives the best recovery result in PSNR which is 34.86dB. The DLMRI method also has a close PSNR of 34.75dB. We also demonstrate in Fig. 7 the comparison with various downsampling factors. When the downsampling factor is within 10 fold, the NLDR performance is comparable to that of the DLMRI method, while the SparseMRI generates much lower recovery PSNRs. When the downsampling factor reaches 20, the reconstructed image PSNR drops drastically for SparseMRI, and the NLDR is 1.15dB less than DLMRI PSNR. The reason that DLMRI performs better than NLDR is that, DLMRI uses dictionary learning to find the best sparse representation basis for each single test image. NLDR naturally utilizes a general DCT basis to represent the original test image. As a universal basis, it is not chosen to be optimal for one image. The DLMRI also has its disadvantages- the recovery time usually lasts for hours for a large image

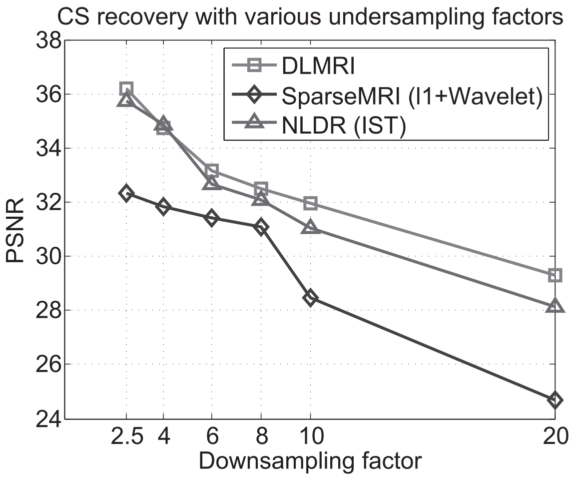

Fig. 7. CS recovery results comparison with various downsampling factors.

as the dictionary learning takes a lot of computations. The computation time needed for NLDR is at the same level as those of TVAL3 and BCS-SPL. For all our test images of size 512×512, NLDR takes, on average, about 10 minutes to finish on a Laptop PC.

V. Conclusion

This paper presented a CS image recovery algorithm based on Douglas-Rachford Splitting with nonlocal estimation. The proposed **NLDR** algorithm first used the iterative thesholding algorithm to obtain the intermediate image reconstruction result. Then a nonlocal estimation step was applied to the reconstructed image to improve the recovery performance. In the nonlocal estimation step, we reformulated the patches estimation as patch denoising problem using low-rank matrix approximation. We proposed a Douglas-Rachford splitting method to solve the CS recovery problem with the nonlocal estimation. Experimental results validated the performance of the proposed NLDR algorithm in both PSNR and visual perception on standard test images with both noiseless and noisy settings. NLDR outperformed the state-of-the-art CS recovery algorithms and showed it can be applied on top of existing recovery algorithms to further improve the recovery performance. Experiments on MRI data also demonstrated it is practical for real applications with competing results.

References

[1] D. L. Donoho, "Compressed sensing," *IEEE Trans. Inf. Theory*, vol. 52, no. 4, pp. 1289–1306, Apr. 2006.

[2] E. J. Candès, J. Romberg, and T. Tao, "Robust uncertainty principles: Exact signal reconstruction from highly incomplete frequency information," *IEEE Trans. Inf. Theory*, vol. 52, no. 2, pp. 489–509, Feb. 2006.

[3] M. Lustig, D. Donoho, and J. M. Pauly, "Sparse MRI: The application of compressed sensing for rapid MR imaging," *Magn. Reson. Med.*, vol. 58, no. 6, pp. 1182–1195, Dec. 2007.

[4] S. Mun and J. E. Fowler, "Block compressed sensing of images using directional transforms," in *Proc. 16th IEEE Int. Conf. Image Process. (ICIP)*, Nov. 2009, pp. 3021–3024.

[5] J. Zhang, D. Zhao, C. Zhao, R. Xiong, S. Ma, and W. Gao, "Compressed sensing recovery via collaborative sparsity," in *Proc. Data Compress. Conf. (DCC)*, Apr. 2012, pp. 287–296.

[6] C. Li, W. Yin, and Y. Zhang. (2009). *TVAL3: TV Minimization by Augmented Lagrangian and Alternating Direction Algorithms*. [Online]. Available: http://www.caam.rice.edu/~optimization/L1/TVAL3/

[7] L. Gan, "Block compressed sensing of natural images," in *Proc. 15th Int. Conf. Digit. Signal Process.*, Jul. 2007, pp. 403–406.

[8] J. Dahl, P. C. Hansen, S. H. Jensen, and T. L. Jensen, "Algorithms and software for total variation image reconstruction via first-order methods," *Numer. Algorithms*, vol. 53, no. 1, pp. 67–92, Jan. 2010.

[9] C. Louchet and L. Moisan, "Total variation as a local filter," *SIAM J. Imag. Sci.*, vol. 4, no. 2, pp. 651–694, 2011.

[10] M. Elad and M. Aharon, "Image denoising via sparse and redundant representations over learned dictionaries," *IEEE Trans. Image Process.*, vol. 15, no. 12, pp. 3736–3745, Dec. 2006.

[11] I. Daubechies, M. Defrise, and C. De Mol, "An iterative thresholding algorithm for linear inverse problems with a sparsity constraint," *Commun. Pure Appl. Math.*, vol. 57, no. 11, pp. 1413–1457, 2004.

[12] I. Daubechies, M. Fornasier, and I. Loris, "Accelerated projected gradient method for linear inverse problems with sparsity constraints," *J. Fourier Anal. Appl.*, vol. 14, nos. 5–6, pp. 764–792, 2008.

[13] A. Buades, B. Coll, and J. M. Morel, "A review of image denoising algorithms, with a new one," *Multiscale Model. Simul.*, vol. 4, no. 2, pp. 490–530, 2005.

[14] G. Peyré, S. Bougleux, and L. Cohen, "Non-local regularization of inverse problems," in *Computer Vision—ECCV*. Berlin, Germany: Springer-Verlag, 2008, pp. 57–68.

[15] Z. Yang and M. Jacob, "Nonlocal regularization of inverse problems: A unified variational framework," *IEEE Trans. Image Process.*, vol. 22, no. 8, pp. 3192–3203, Aug. 2013.

[16] J. Zhang, S. Liu, D. Zhao, R. Xiong, and S. Ma. (2012). "Improved total variation based image compressive sensing recovery by nonlocal regularization." [Online]. Available: http://arxiv.org/abs/1208.3716

[17] X. Shu, J. Yang, and N. Ahuja, "Non-local compressive sampling recovery," in *Proc. IEEE Int. Conf. Comput. Photography (ICCP)*, May 2014, pp. 1–8.

[18] W. Dong, G. Shi, X. Li, Y. Ma, and F. Huang, "Compressive sensing via nonlocal low-rank regularization," *IEEE Trans. Image Process.*, vol. 23, no. 8, pp. 3618–3632, Aug. 2014. AQ:3

[19] G. Chierchia, N. Pustelnik, B. Pesquet-Popescu, and J.-C. Pesquet, "A nonlocal structure tensor-based approach for multicomponent image recovery problems," *IEEE Trans. Image Process.*, vol. 23, no. 12, pp. 5531–5544, Dec. 2014.

[20] X. Zhang, M. Burger, X. Bresson, and S. Osher, "Bregmanized nonlocal regularization for deconvolution and sparse reconstruction," *SIAM J. Imag. Sci.*, vol. 3, no. 3, pp. 253–276, 2010.

[21] S. Osher, M. Burger, D. Goldfarb, J. Xu, and W. Yin, "An iterative regularization method for total variation-based image restoration," *Multiscale Model. Simul.*, vol. 4, no. 2, pp. 460–489, 2005.

[22] E. J. Candès and T. Tao, "The power of convex relaxation: Near-optimal matrix completion," *IEEE Trans. Inf. Theory*, vol. 56, no. 5, pp. 2053–2080, May 2010.

[23] W. Dong, G. Shi, and X. Li, "Nonlocal image restoration with bilateral variance estimation: A low-rank approach," *IEEE Trans. Image Process.*, vol. 22, no. 2, pp. 700–711, Feb. 2013.

[24] H. Ji, C. Liu, Z. Shen, and Y. Xu, "Robust video denoising using low rank matrix completion," in *Proc. IEEE Conf. Comput. Vis. Pattern Recognit. (CVPR)*, Jun. 2010, pp. 1791–1798.

[25] J. Douglas and H. Rachford, "On the numerical solution of heat conduction problems in two and three space variables," *Trans. Amer. Math. Soc.*, vol. 82, no. 2, pp. 421–439, 1956.

[26] P. L. Combettes and J.-C. Pesquet, "Proximal splitting methods in signal processing," in *Fixed-Point Algorithms for Inverse Problems in Science and Engineering*. Berlin, Germany: Springer-Verlag, 2011, pp. 185–212.

[27] P. L. Combettes and V. R. Wajs, "Signal recovery by proximal forward-backward splitting," *Multiscale Model. Simul.*, vol. 4, no. 4, pp. 1168–1200, 2005.

[28] *Software ℓ_1-Magic*. [Online]. Available: http://users.ece.gatech.edu/~justin/l1magic/, accessed Aug. 23, 2014.

[29] J. Zhang, S. Liu, R. Xiong, S. Ma, and D. Zhao, "Improved total variation based image compressive sensing recovery by nonlocal regularization," in *Proc. IEEE Int. Symp. Circuits Syst. (ISCAS)*, May 2013, pp. 2836–2839.

[30] K. Dabov, A. Foi, V. Katkovnik, and K. Egiazarian, "Image denoising by sparse 3D transform-domain collaborative filtering," *IEEE Trans. Image Process.*, vol. 16, no. 8, pp. 2080–2095, Aug. 2007.

[31] (2009). *American Radiology Services*. [Online]. Available: http://www3.americanradiology.com/pls/web1/wwimggal.vmg

[32] S. Ravishankar and Y. Bresler, "MR image reconstruction from highly undersampled k-space data by dictionary learning," *IEEE Trans. Med. Imag.*, vol. 30, no. 5, pp. 1028–1041, May 2011.

Shuangjiang Li received the B.S. degree in electrical engineering from the University of Science and Technology Beijing, Beijing, China, in 2009, and the M.S. and Ph.D. degrees in computer engineering from the University of Tennessee, Knoxville, TN, in 2011 and 2015, respectively. His research interests include signal and image processing, compressed sensing, mobile sensing systems, and WSN.

Hairong Qi (S'97–M'00–SM'05) received the B.S. and M.S. degrees in computer science from Northern JiaoTong University, Beijing, China, in 1992 and 1995, respectively, and the Ph.D. degree in computer engineering from North Carolina State University, Raleigh, in 1999.

She is currently the Gonzalez Family Professor with the Department of Electrical Engineering and Computer Science, University of Tennessee, Knoxville. Her current research interests are in advanced imaging and collaborative processing in resource-constrained distributed environment, hyperspectral image analysis, and automatic target recognition.

Dr. Qi was a recipient of the NSF CAREER Award. She also received the Best Paper Awards at the 18th International Conference on Pattern Recognition in 2006, the third ACM/IEEE International Conference on Distributed Smart Cameras in 2009, and the Seventh IEEE Workshop on Hyperspectral Image and Signal Processing: Evolution in Remote Sensor in 2015. She received the Highest Impact Paper from the IEEE Geoscience and Remote Sensing Society in 2012.

AUTHOR QUERIES

AQ:1 = Please confirm whether the corresponding author information is correct as set.

AQ:2 = Please note that some figures and tables are placed before their first citations in order to avoid having figures appear in the conclusion and references sections, which would be against IEEE style. Please confirm that the placement of all figures and tables are fine.

AQ:3 = Please note that references [18] and [20] are the same. Hence we deleted Ref. [20] and renumbered the other references. This change will also reflect in the citations present in the body text. Please confirm.